

Department of Precision and Microsystems Engineering

Resetting Velocity Feedback: Reset Control for Active Damping

Mathew Antony Mohan

Report no : 2021.043
Coach : M. B. Kaczmarek
Professor : S. H. Hossein Nia
Specialisation : Mechatronic System Design
Type of report : Master Thesis
Date : 19 July 2021

RESETTING VELOCITY FEEDBACK

RESET CONTROL FOR ACTIVE DAMPING

RESETTING VELOCITY FEEDBACK

RESET CONTROL FOR ACTIVE DAMPING

Master Thesis

for the purpose of obtaining the M.Sc. Degree
at the Delft University of Technology

by

Mathew. A. MOHAN

Department of Precision and Microsystems Engineering
Faculty of Mechanical, Maritime, and Materials Engineering (3mE)
Delft University of Technology
The Netherlands

This thesis has been approved by

Supervisor: Dr. S.H.Hossein Nia Kani

Daily Supervisor: M. B. Kaczmarek

Composition of the committee:

Dr. S.H, Hossein Nia Kani, Technische Universiteit Delft

M.B. Kaczmarek, Technische Universiteit Delft

Independent Members:

Dr. M. Jafarian Technische Universiteit Delft

Dr. A. Hunt Technische Universiteit Delft

An electronic version of this dissertation is available at

<http://repository.tudelft.nl/>

The miracle of the appropriateness of the language of mathematics for the formulation of the laws of physics is a wonderful gift which we neither understand nor deserve. We should be grateful for it and hope that it will remain valid in future research and that it will extend, for better or for worse, to our pleasure, even though perhaps also to our bafflement, to wide branches of learning.

Eugene Wigner

CONTENTS

Abstract	ix
Acknowledgements	xi
Preface	xiii
1 Introduction	1
1.1 Outline	2
2 Literature Review	3
2.1 Active Damping	3
2.1.1 Dynamics of flexible structures	3
2.1.2 Collocation and duality	4
2.1.3 Linear Active Damping Methods	5
2.2 Motivation for Hybrid Damping Controllers	8
2.3 Hybrid Control for Active Damping - Resetting Virtual Absorbers	9
2.3.1 Underlying Controller Principle	11
2.4 Reset Control	12
2.4.1 Reset Control in Frequency Domain	14
3 Research Gap and Objectives	21
4 Resetting Velocity Feedback: Reset Control for Improved Transient Damping	23
4.1 Introduction	24
4.2 Preliminaries	25
4.2.1 Reset Control and Describing Functions	26
4.2.2 Negative Derivative Feedback	28
4.2.3 Resetting Virtual Absorbers	28
4.3 Framework	30
4.3.1 From RVA to RVF	30
4.3.2 Stability Analysis	34
4.4 Results	35
4.4.1 Sensitivity Analysis	39
4.5 Conclusions and Future Work	40
5 Conclusion	43
6 Appendix A	45
7 Appendix B	51

ABSTRACT

As the age of digitization evolves rapidly, there is an ever-increasing demand for improving precision and decreasing production times for industrial automation in general, and semiconductor manufacturing in particular. As these complex machines incorporate flexural elements to overcome friction and backlash, structural vibrations pose a new challenge. Hence the need for controlling and quickly damping these vibrations are paramount. In this thesis, a novel reset-based bandpass filter that employs velocity feedback to achieve finite-time vibration suppression for damped systems is introduced. The development of this filter stems from an energy based mechanistic approach, providing a clear understanding of the underlying mechanism for the improved transient response, which also motivates the use of reset. Systematic tuning rules based on describing functions are also developed to enable design in the frequency domain, thereby increasing its relevance for industries. Finally, the effectiveness of the Resetting Velocity Feedback framework for improved transient damping is demonstrated experimentally on a single degree-of-freedom flexure stage. The results are compared to a linear bandpass filter and validates the advantages of reset control for achieving better transient damping compared to linear control.

ACKNOWLEDGEMENTS

This thesis is based on the research conducted at the Department of Precision and Microsystems Engineering, TU Delft. I am grateful to God, a number of friends and colleagues, and my family who helped me through this journey.

I had the great pleasure of having Marcin as my daily supervisor. Marcin was patient, dedicated, helpful, and overall a fantastic coach during the duration of this thesis. In addition to this, I was also very lucky to have Hassan as my main supervisor. The relevant questions he raised during our monthly meetings has ensured the scientific rigor of the work presented. More importantly, I am indebted to him for giving me the freedom to explore new and novel topics, and the autonomy to shape my research topic and questions gradually as I went along.

I was very lucky to have help from other distinguished members of the faculty as well. Jo Spronck gave his valuable practical insights regarding setting up experiments. I am also immensely grateful to Nima Karbasizadeh for his invaluable insights and support in helping me setting up LabVIEW for my experiments. I also thank the Lab Support technicians who helped me in acquiring all the necessary hardware for my experiments.

I express my gratitude to my peers: Thomas, Roelof, Romano, and Hani for helping me with troubleshooting experimental issues, but more importantly for making work fun.

Last, but certainly not least, I am forever indebted to my family - my parents and my sister who were always supportive of my decisions, and were a constant source of motivation and inspiration during the entirety of my student years.

PREFACE

This chapter serves as a guide for readers on how to efficiently go through the contents of this Thesis by providing an overview of what to expect in the coming pages.

Chapter 1 provides an introduction to the thesis and sets the stage for the research problem at hand, by motivating the need for active damping in general, and hybrid control for active damping in particular.

Chapter 2 provides the necessary background on existing linear active damping methods, motivates the need for nonlinear hybrid control in active damping, and introduces the foundations of one such hybrid control method - reset control.

Once the background and state-of-the art methods are studied, the research gap and research objectives will be established in Chapter 3.

Chapter 4 is presented in a conference/journal paper format. This forms the crux of this Thesis. This chapter is self-contained and should provide the reader with an introduction to the problem, the background information to understand the research, experimental results of the research conducted, and conclusions and recommendations for future work. If you are short on time, I would recommend reading this chapter alone, as it includes the entirety of the research conducted.

Chapter 5 concludes the study and briefly summarizes the contributions

For readers who are interested in replicating/extending the experimental study, the Appendices might be of interest.

Appendix A contains the MATLAB code for obtaining the describing function of the proposed reset bandpass filter, and generating the FRFs from experimental data. Parts of the former is adopted from the M.Sc. Thesis of Kars Heinen (2018) at TU Delft.

Appendix B gives a comprehensive treatment of the experimental setup, the components used, its important technical specifications, and most importantly, certain tips on how to perform experiments effectively. This includes but are not limited to, what settings to choose for different components, which software versions to install for seamless integration, installation instructions, the basic structure of a LabVIEW FPGA program and an elaborate treatment of the experimental method. This might be beneficial for someone who intends to replicate the results or extend the study further and plans to use a similar setup.

I hope you find this preface useful and effective to optimize your time and energy spent in understanding and appreciating the contents of this document.
Happy reading!

*Mathew Mohan
Delft, July 2021*

1

INTRODUCTION

There are ever-increasing demands on both the accuracy and the throughput of high-precision machines. Examples of such machines are lithographic wafer scanners for the semi-conductor industry, scanning microscopes, and metrology systems like coordinate measuring machines (CMMs). As these machines are designed to be light and prevent friction and backlash, they employ flexure-based designs. Such designs unavoidably introduces structural flexibility and vibrations. Aggressive set points are usually used to increase the throughput of such machines. This leads to large reaction forces exerted on the machine frames and, subsequently, heavy vibrations are induced by the machine itself. This is a huge concern in the precision and automation industries. To maintain the accuracy levels needed for precision manufacturing, one has to wait for such vibrations to settle, which ironically reduces the machine's throughput. Hence, transient damping performance becomes a key-factor in the performance of these machines.

Vibration damping techniques aim to suppress the resonant vibrations of flexible structures by adding damping into these structures. They can be broadly classified into:

Passive Damping methods add damping to the structure by introducing additional passive components like tuned-mass dampers, constrained-layer damping, magnetic damping etc. These methods tends to add extra mass to the system and is not very easy to tune for parametric variations, in case of a tuned-mass damper.

Semi-active Damping methods usually add damping to the structure using active elements such as piezoelectric shunt circuits and magnetorheological dampers to effectively dissipate vibration energy. In case of shunting circuits, this might at times result in extremely large inductors. Furthermore, tune-ability is again an issue with such methods.

Active Damping methods use sensors, actuators, and a feedback control loop to effectively suppress vibrations of structures. These have the benefits of very low added mass (depending on the choice of sensors and actuators) and ease of tune-ability since it employs digital control design. Another advantage of such techniques that is less commonly addressed is the ability to alter the mode shapes of the structure [17, 18]. By cleverly placing the sensor-actuator pairs, and tuning the controller, it is possible to change

the mode shapes of the structure. This is particularly important if there are vibration sensitive equipments on board. By careful placement and tuning, these can be located at the vibration nodes of the structure, and hence be locally isolated from vibrations.

Due to these advantages, active damping techniques are widely used in practice in aerospace, automotive, precision, and automation industries. Active damping techniques can be further classified into:

Non-modal techniques provides damping across the entire range of actuator bandwidth. These were the first active damping techniques to be introduced for lightweight flexible structures [Balas, 1979] and is now known as Direct Velocity Feedback (DVF or DVFB). However, when the objective of active damping is to suppress the resonant vibrations of the structure, such an approach is highly inefficient as the actuator energy is spread across a broad range of frequencies, making it highly energy inefficient.

Modal active damping techniques were introduced to tackle this issue. In such techniques, the controller is a dynamic element with a certain filter behaviour. These are usually tuned to one or more modes of the structure, and allows the actuators to concentrate their energy to these particular frequencies. These also tackle the problem of instability and spillover, as mentioned in Chapter 2. The key idea of all modal damping controllers is to provide a feedback signal proportional to the modal velocity, but opposite in phase. This provides damping to the structure.

Existing state-of-the-art active damping techniques use linear feedback control to actively damp these vibrations. However, certain nonlinear techniques seems to hold high promise to achieve better transient performance than these linear techniques, while being easy to design and implement.

The aim of this research thesis is to develop a nonlinear hybrid vibration control technique that is easy to design and implement using frequency-domain analysis tools and investigate if considerable transient damping performance gains can be achieved over linear techniques, while ensuring robustness to plant variations. Furthermore, practical implementation and challenges that arise with this novel controller will also be investigated.

1.1. OUTLINE

The outline of this thesis is as follows:

- Chapter 2 provides the necessary background on existing linear active damping methods, motivates the need for nonlinear hybrid control in active damping, and introduces the foundations of one such hybrid control method - reset control
- Once the background and state-of-the art methods are studied, the research gap and research objectives will be established in Chapter 3
- With the research objectives identified, the main contributions of this thesis will be presented in Chapter 4. This is presented in a journal paper format, and includes the development of the framework, and the numerical and experimental results
- Chapter 5 concludes the study and briefly summarizes the contributions

2

LITERATURE REVIEW

This chapter provides a review of the relevant literature for the remainder of this thesis. In Section 2.1, the foundations of dynamics and linear control for active damping of flexible structures are introduced. Section 2.2 provides a motivation to move beyond linear control techniques and explore nonlinear hybrid control techniques for active damping controllers. This is further illustrated in Section 2.3 which analyses Resetting Virtual Absorbers. This is a hybrid control technique that uses reset action to inject damping into undamped systems. After demonstrating the effectiveness of reset, Section 2.4 provides a comprehensive overview of reset control in both time- and frequency-domains.

2.1. ACTIVE DAMPING

2.1.1. DYNAMICS OF FLEXIBLE STRUCTURES

Flexible mechanical structures are distributed parameter systems. This means they have an infinite number of flexible modes [Balas, 1979]. Therefore, to completely describe their dynamic response we would need infinite degrees of freedom. However, for practical purposes like modelling and control, the vibration characteristics of these systems can be approximated by a finite number of flexible modes resulting in a lumped parameter system. These modes can be obtained by finite-element modelling, modal analysis or system identification [Moheimani and Fleming, 2006]. Once these modes are obtained, they can be expressed in the frequency domain through Fourier transforms. Mathematically, the transfer function from the force input to the displacement output of the lumped parameter system G can be expressed in the frequency domain as the sum of M modes by

$$G = \sum_{i=1}^M \frac{\omega_i^2}{s^2 + 2\zeta_i \omega_i s + \omega_i^2} \quad (2.1)$$

where ζ_i and ω_i corresponds to the damping ratio and eigenfrequency of the i th flexible mode, and s is the Laplace variable. A more accurate model which accounts for the truncated flexible modes, also called as residual modes is defined as [Preumont, 1999]

$$G = \sum_{i=1}^M \frac{\omega_i^2}{s^2 + 2\zeta_i \omega_i s + \omega_i^2} + R \quad (2.2)$$

where R is the effect of residual modes. The effect of R in frequency domain is a constant static gain for all frequencies [Holterman, 2002]. This feed-through term is often essential to model the system well, especially when using feedback controllers that use collocation [Moheimani and Fleming, 2006].

Such a description effectively allows us to treat a continuous flexible structure as a collection of independent mass-spring-damper systems and develop active damping techniques for each of these independent systems.

2.1.2. COLLOCATION AND DUALITY

Collocated systems are systems where sensors and actuators are attached to the same degree of freedom of the system. In practice, this is realized by having the sensor-actuator pair at the same location. Duality refers to the sensing and actuating variable pair, whose product should equal the energy transfer (for example, position sensing and force actuation, or angular position and moment actuation). Perfectly collocated and dual systems enjoy an interesting property that their poles and zeros interlace, and their phase always lies between 0 and -180 degrees, as shown in Figure 2.1. This makes them unconditionally stable even in the presence of out-of-bandwidth dynamics, as long as there are no additional controller, actuator, and filter dynamics. In a collocated system, the FRF from the actuator to the sensor for the i th mode is represented by

$$G = \frac{\phi_i^2}{s^2 + 2\zeta_i \omega_i s + \omega_i^2} \quad (2.3)$$

where ϕ_i is the modal displacement at the actuator/sensor location.

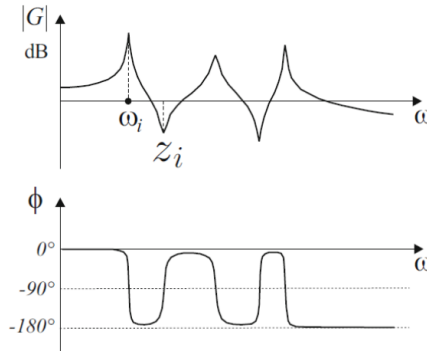


Figure 2.1: Bode plot of a lightly damped collocated system [Preumont, 1999]

Perfect collocation is very difficult to achieve, unless we have a self-sensing actuator. In most cases, the actuator and sensor are placed very close to each other to give rise to nearly collocated setups. As long as both the actuator and the sensor have the same sign

for modal displacement, and similar magnitudes, these systems shows the similar stability and robustness properties. Hence for practical purposes, this is usually preferred.

2.1.3. LINEAR ACTIVE DAMPING METHODS

A variety of active damping methods exist. In this section some of these methods will be briefed upon. Broadly speaking, active damping controllers can be modal or non-modal controllers. Non-modal controllers do not target to damp a particular mode of the system. Direct Velocity Feedback (DVF) is an example of such a controller. Modal controllers are designed and tuned to damp certain modes of the system. These include Positive Position Feedback (PPF) and Negative Derivative Feedback (NDF).

DIRECT VELOCITY FEEDBACK

Historically, one of the first active damping methods used for structural vibrations was Direct Velocity Feedback (DVF), by Balas [Balas, 1979]. In this method, the structural velocity of vibration is fed back in a negative fashion, thereby introducing damping to the structure. Schematically this is represented in Figure 2.2, where the velocity signal is amplified by a gain g .

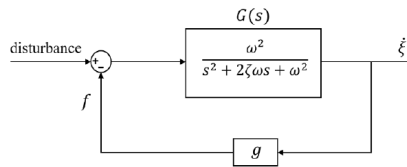


Figure 2.2: Block diagram of Direct Velocity Feedback

This was initially reported to be unconditionally stable for all positive gain values, but [GOH and CAUGHEY, 1985] later proved otherwise. When actuators have a finite bandwidth (as is the case, always), modes above this bandwidth could go unstable. Furthermore, DVF is a non-modal damping approach. This means that the control energy is used throughout the actuator bandwidth, thereby making it highly inefficient. To overcome these issues, Positive Position Feedback (PPF) was introduced.

POSITIVE POSITION FEEDBACK

Introduced by Fanson and Caughey, [Fanson and Caughey, 1990] in PPF position which is positively feedback through a second order filter, resembling the dynamics of the plant. In essence, a PPF filter is a second order low-pass filter, tuned to the natural frequency of the mode to be suppressed, which provides effective damping at this target frequency. The structure PPF is shown in Figure 2.3. For the single DOF plant

$$\ddot{q} + 2\zeta_c \omega_p \dot{q} + q\omega_p^2 = f \quad (2.4)$$

The PPF compensator dynamics is represented by

$$\ddot{\eta} + 2\zeta_c \omega_c \dot{\eta} + \eta\omega_c^2 = q\omega_c^2 \quad (2.5)$$

The control action generated by the PPF controller is

$$f = g\eta \quad (2.6)$$

ω_c is usually chosen equal to ω_p . g denotes the PPF gain, and ζ_c denotes the damping ratio of the compensator. A lower value of ζ_c provides a higher control force.

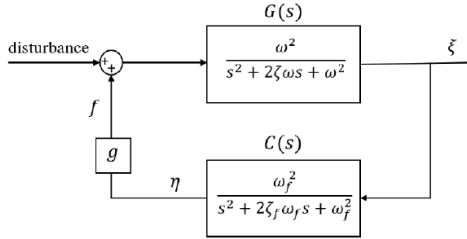


Figure 2.3: Block diagram of Positive Position Feedback

PPF is not unconditionally stable, and as mentioned in [Preumont, 1999] $g > 1$ shifts the closed loop poles to the RHP. Another limitation of PPF is its low-frequency spillover. The high DC gain of the low pass filter alters the frequency of all modes with a frequency lower than ω_c . This makes PPF tuning for multi-modal situations difficult as higher modes need to be damped first. It also introduces a steady-state position error, which manifests as increased steady-state gain as shown in Figure 2.4. This issue can be reduced by using a fractional-order PPF filter [Marinangeli, 2016]. In [Creasy et al., 2008] a bandpass filter was added to PPF to eliminate low-frequency spillover. However, adding a bandpass filter in series with PPF requires re-tuning of the PPF filter, and also results in a marginally worse resonant damping performance. In [citePPFtuning], a comprehensive PPF tuning strategy was developed for maximum damping, using an \mathcal{H}_2 optimization approach, for damping a single mode.

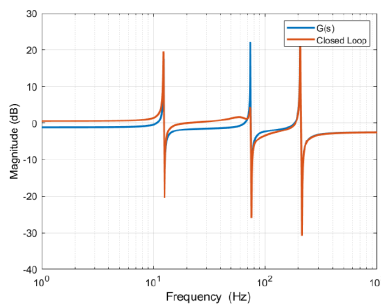


Figure 2.4: Damping the second mode using PPF results in low frequency spillover and increased static gain

NEGATIVE DERIVATIVE FEEDBACK

In [Cazzulani et al., 2012] Negative Derivative Feedback (NDF) was introduced to overcome the spillover and stability limitations of PPF. In NDF, velocity is fed back negatively

though a linear second-order bandpass filter, tuned to ω_c . The compensator is represented by

$$\ddot{\eta} + 2\zeta_c \omega_c \dot{\eta} + \eta \omega_c^2 = k(\dot{q} - \dot{\eta}) \tag{2.7}$$

the control force being

$$f = -\dot{\eta} \tag{2.8}$$

The block diagram representation is given in Figure 2.5 . The bandpass characteristics of NDF prevent spillover at low and high frequencies. Unlike PPF, increasing the gain g above unity does not result in instability. This gives more design freedom and, as stated in [Cazzulani et al., 2012], better damping performance compared to PPF.

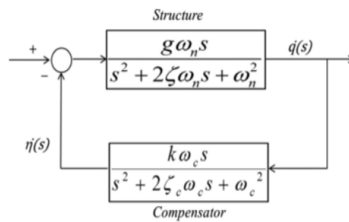


Figure 2.5: Block diagram of Negative Derivative Feedback [Cazzulani et al., 2012]

The main advantage of using such bandpass filters is that they act as modal filters [Kim and Oh, 2013]. Each modal filter of second order is designed to be sensitive to the target mode for control, while insensitive to the others. This is shown in Figure 2.6 where two bandpass filters are used in parallel for active damping of two structural modes. This means they can be effectively used for both collocated as well as non-collocated control. In case of out-of-phase modes that result from non-collocation, a positive feedback strategy can be employed instead of negative feedback, and effective damping can be achieved. Using non-collocated control over collocated control also comes with additional benefits. Non-collocated plants generally exhibit better high-frequency roll-off characteristics because there are weaker mechanical and electrical feed-through couplings between non-collocated transducers.

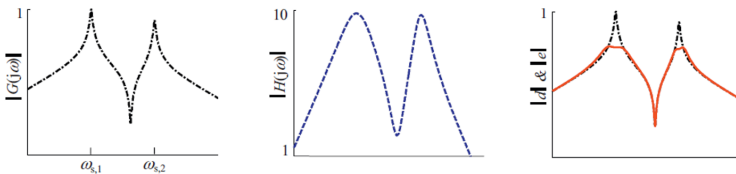


Figure 2.6: Two NDF filters in parallel $H(j\omega)$ are used to damp two modes of the structure $G(j\omega)$ without spillover [Kim and Oh, 2013]

2.2. MOTIVATION FOR HYBRID DAMPING CONTROLLERS

The controllers discussed so far were linear controllers. As these are designed in the frequency domain using frequency response functions, they do not explicitly take transient damping performance into account. This begs the question: can nonlinear control techniques improve active transient damping performance of flexible structures?

Nonlinear control techniques include feedback linearization, adaptive control, control laws based on passivity and Control Lyapunov Functions etc. These control techniques generate smooth nonlinear feedback laws, and the state trajectories are continuously differentiable. Hybrid control is a class of nonlinear feedback control which uses a class of feedback laws and a switching logic, to switch between the feedback laws. This introduces discrete dynamics along with continuous dynamics, hence the term 'hybrid' control. This discrete nature and switching action results in trajectories that are non-smooth and non-differentiable, which could be advantageous in certain instances.

The interest in hybrid control comes from multiple sources. For one, hybrid feedback can be used to provide efficient solutions to local and global feedback stabilization problems that cannot be solved by classical feedback control [Astolfi et al., 2008]. In addition, the added flexibility of hybrid control sometimes allows the designer to achieve closed-loop responses not possible with classical linear and smooth nonlinear feedback control. A case in point is that for a double integrator system to have zero-steady state error, it is proven that the response must overshoot. However, with hybrid control it is possible to achieve zero steady-state error without overshoot [Feuer et al., 1997]. Hybrid control can also show properties of the multiple independent feedback laws [Astolfi et al., 2008].

One of the most well-known hybrid control strategies to improve the transient performance of linear (motion) systems is reset control. A reset controller is an LTI control system of which the state, or a subset of the state is reset to a certain value (usually zero) whenever appropriate algebraic conditions on its input and output are satisfied. Reset control has its origin in 1958 by the introduction of the so-called Clegg integrator. The Clegg integrator was proposed to overcome the inherent performance limitation in LTI control related to a balance between settling time and overshoot. For example, tracking in linear systems is always a trade-off between a fast-response and high overshoot, versus a slower response to achieve lower overshoot. This can be overcome using reset control as illustrated in Figure 2.7. Reset control produces zero overshoot for the same rise-time for tracking.

Another hybrid control strategy that focuses on the integral action of the controller in order to improve the transient performance is given in [Feuer et al., 1997], in which a switched integral controller is proposed for an LTI plant consisting of an integrator. In [M. F. Heertjes and Vardar, 2013], a sliding mode controller with a saturated integrator is studied, which essentially switches between proportional-derivative (PD) control and proportional-integral-derivative (PID) control in order to limit the overshoot while still achieving a zero steady-state error. In a similar context, the concept of composite nonlinear feedback in [Lin et al., 2011] combines two linear control laws with a nonlinear tuning function to improve the transient response of second-order LTI systems. Hybrid Integrator Gain Switching (HIGS) was developed by [Deenen et al., 2017], which used a switching logic to switch between an integrating mode and a proportional mode. Such

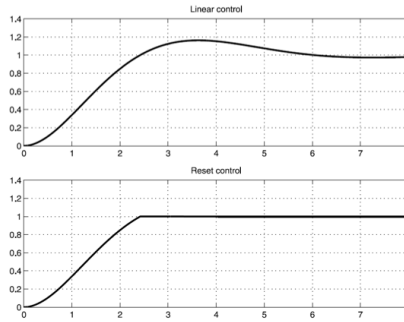


Figure 2.7: Response to a step input with a linear and reset controller. Reset controller results in a similar rise time with zero overshoot [Guo et al., 2015]

a controller showed phase advantages in the frequency domain similar to reset control. This has been used to improve tracking, transient response, and disturbance attenuation. In [M. Heertjes et al., 2019], a HIGS-based bandpass filter was developed for active vibration isolation, to improve transient damping performance.

The abundance of existing literature which shows that hybrid control can improve transient performance is what motivates the use of hybrid control for active damping.

As opposed to linear controllers, the design and tuning of hybrid controllers is often rather complex and requires additional expertise of the control engineer. In this context, it is important to mention that control engineers (in industry) are often used to analyzing performance, and to design stabilizing controllers, based on ‘linear’ frequency-domain characteristics of a closed-loop control system, such as the sensitivity function and complementary sensitivity function. Often, the design and analysis of hybrid controllers requires accurate parametric models and solving linear matrix inequalities (LMIs), which, from an industrial point-of-view, introduces considerable design complexity and is not easily embraced.

2.3. HYBRID CONTROL FOR ACTIVE DAMPING - RESETTING VIRTUAL ABSORBERS

The concept of a resetting virtual absorber is based on the insightful analysis found in [R. T. Bupp et al., 2000, R. Bupp et al., 1996] which shows how reset can inject damping into an undamped system consisting of a single degree-of-freedom oscillator and an emulated vibration absorber, for finite-time vibration suppression.

Consider a single degree-of-freedom undamped oscillator with mass M and stiffness K , in series with an emulated dynamic vibration absorber with mass m and stiffness k , whose states (position and velocity), can be instantaneously reset to zero. This is shown in Figure 2.8. This emulated vibration absorber can be considered an active damping controller, which uses the position of mass M as its input [Kim and Oh, 2013]. As a block diagram, this can be represented as shown in Figure 2.9 (the diagonal arrow denotes a reset element).

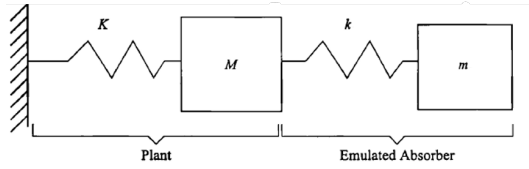


Figure 2.8: The model of a Resetting Virtual Absorber [R. Bupp et al., 1996]

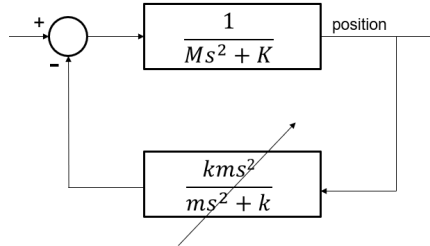


Figure 2.9: Block diagram representation of the RVA framework

For an impulse excitation to mass M , for $m = 1.33M$ and $k = 1.33K$ [R. Bupp et al., 1996], the response of the system is shown in Figure 2.10. When the position of mass M reaches zero for the first time, the velocities of masses M and m are also simultaneously zero, as indicated in Figure 2.10. Therefore, the energy contained in the system at this instant is uniquely due to the compression of spring k , i.e., the non-zero position of mass m . In other words, all the energy is contained within the emulated absorber.

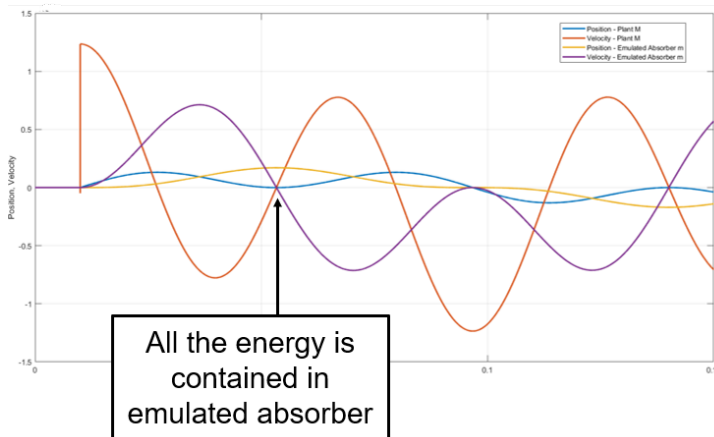


Figure 2.10: Response of the system in Figure 4.5 to an impulse excitation on mass M

If the states (virtual position and velocity) of the emulated absorber (controller) are reset to zero at this exact instant, the total energy in the system is instantaneously dissipated before it redistributes it to the states of mass M . Hence, damping is injected into the system by resetting the states of the controller. This results in finite-time suppression

of the oscillations of mass M , as shown in Figure 2.11. Reset is the only source for damping as this system has no natural damping whatsoever. The control effort is the force provided by the compression of spring k and can be seen to follow a smooth trajectory until the point where the position of mass M hits zero. It is then instantaneously reset to zero as shown in Figure 2.11.

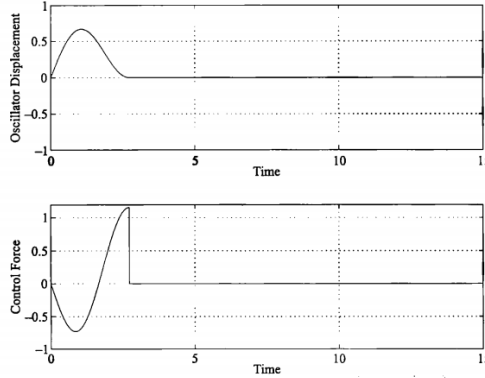


Figure 2.11: Finite-time vibration suppression using RVA [R. Bupp et al., 1996]

2.3.1. UNDERLYING CONTROLLER PRINCIPLE

Further insight into the underlying controller principle can be obtained by analyzing the system in Figure 2.8 from its equations of motion.

The equation of motion for mass M is given by

$$Ms^2X_1 + KX_1 = u \quad (2.9)$$

where X_1 is the position of mass M in the laplace domain, s is the laplace variable and u is the force exerted by spring k given by

$$u = k(X_2 - X_1) \quad (2.10)$$

where X_2 is the absolute displacement of mass m . Similarly, the equation of motion for mass m is

$$ms^2X_2 + k(X_2 - X_1) = 0 \quad (2.11)$$

From this X_2 can be obtained as follows

$$X_2 = \frac{kX_1}{ms^2 + k} \quad (2.12)$$

Substituting this in equation 2.9, we have

$$\frac{u}{X_1} = \frac{-kms^2}{ms^2 + k} \quad (2.13)$$

This represents the transfer function of the emulated absorber, with X_1 as the input (position feedback) and u as the control output. Therefore, we see that this is a Negative Position Feedback (NPF) controller with high-pass filter characteristics, whose states can be reset to zero when a condition is met (in this case when $X_1 = 0$). Schematically this is shown as a block diagram in Figure 2.9. Note that in [R. Bupp et al., 1996] the reset instants were not specified by analyzing the states, but rather the time instant when $X_1 = 0$, which was found analytically. However, in the framework of reset control, state-based resets are more common, as they are more well-studied [Guo et al., 2015]. Hence we will be adopting such an approach in Chapter 4.

Although the structure Resetting Virtual Absorbers is that of an NPF controller, we see that the damping response as shown in Figure 2.11 is not of that of a linear controller, since it achieves finite-time stabilization. Reset action provides this improvement in damping performance, and the main idea of this thesis will be to see if such controllers can be used for active damping of flexible structures.

2.4. RESET CONTROL

Reset control is a class of hybrid control techniques governed by continuous and discrete dynamics. Such systems in hybrid dynamical system theory is also referred to as Jump-Flow systems.

The first ever reset control strategy was proposed by J.C. Clegg in 1958 [Clegg, 1958] and was called the Clegg Integrator (CI). A CI used an analogue electronics circuit (Figure 2.12) with a switching logic to ensure that the input and output always has the same sign. Mathematically, this meant that the product of the input and output signals of a CI was always positive, as described below

$$\begin{cases} \dot{x}_c = \frac{1}{RC} e, & \text{is allowed when } x_c e \geq 0 \\ x_c^+ = 0, & \text{is allowed when } x_c e \leq 0 \end{cases} \quad (2.14)$$

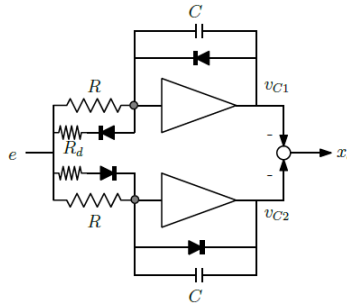


Figure 2.12: A Clegg Integrator circuit [Prieur et al., 2018]

Lets call the first equation of Equation 2.14 the “flow” equation and its second equation the “jump” equation. The two conditions at the right hand side become then the “flow” condition and the “jump” condition. At any time, a solution to the hybrid system may then flow or jump depending on whether its value at that time belongs to the so-

called “jump set”, \mathcal{J} (namely, the set of states for which the jump condition is true) or it belongs to the “flow set”, \mathcal{F} .

An intuitive way to interpret the dynamics is to regard it as a linear filter with a pole at the origin embedded with a special resetting rule dependent on the value of the input and output of the filter at each time. The fact that e and x_c always has the same sign is fundamental to the idea that such a reset element reduces phase lag, compared to a linear counterpart.

With the slow adaptation of digital control systems, the reset condition specified by Clegg depending on the input and output having the same sign got diluted. A new formulation was adopted based on logic arguments, easier to implement in digital controllers given by Equation 2.15

$$\begin{cases} \dot{x}_c = a_c x_c + b_c e, & \text{if } e \neq 0 \\ x_c^+ = 0, & \text{if } e = 0 \end{cases} \quad (2.15)$$

Although this initially looks the same, the state-space formulation reveals subtle difference in flow and jump sets as shown in Figure 2.13. The new formulation in Equation 2.15, leads to “thin” jump sets which results in inferior robustness properties as opposed to the original model. This leads to more conservative stability proofs, and is an active field of research [Priour et al., 2018]. In this thesis we will be analyzing the model given by Equation 2.16. A general description of such a reset element can be given in state-space form as

$$\begin{cases} \dot{x}_c = Ax_c(t) + Be(t), & \text{if } e \neq 0 \\ x_c^+ = 0, & \text{if } e = 0 \\ y(t) = Cx_c(t) + D \end{cases} \quad (2.16)$$

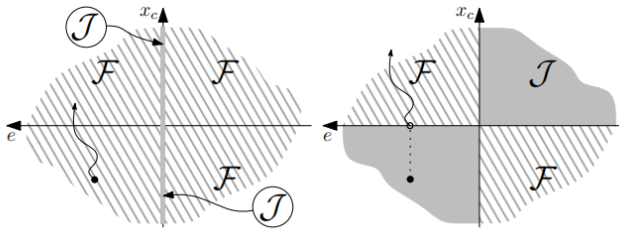


Figure 2.13: The jump (grey) and flow (striped) sets for the revised model (left), and original model (right) proposed by Clegg [Priour et al., 2018]

The time-domain response of such an integrator is shown in Figure 2.14. As can be seen, whenever the input crosses zero, the output of the CI resets to zero. At all other instances, it follows a similar trajectory as a linear integrator. It is also worth noting that the reset action ensures the output and the input has the same sign at all times. This leads to lower inertia of the integrator.

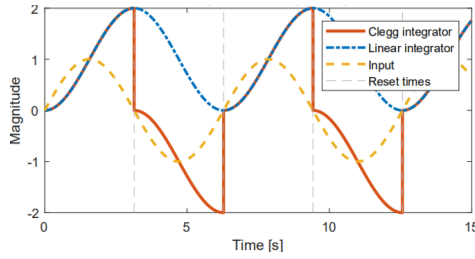


Figure 2.14: The output of a Clegg integrator compared to a linear integrator for a sinusoidal input

2.4.1. RESET CONTROL IN FREQUENCY DOMAIN

SINUSOIDAL INPUT DESCRIBING FUNCTIONS

Linear controllers are mostly designed using frequency domain techniques such as loop shaping. For this, the transfer functions of the controllers are represented in the frequency domain as Frequency Response Functions (FRFs). Similarly, a Describing Function (DF) is a quasi-linearization of a nonlinear element subject to certain excitation input used to approximately analyze the behavior of nonlinear systems. DF is a powerful tool in investigating behaviors of elements with hard non-linearities including dead zone, backlash, and hysteresis, and has been applied in limit cycle prediction and control design [Vidyasagar, 1993].

The Sinusoidal Input DF (SIDF), which uses sinusoidal inputs as excitation signals, is most widely used [Saikumar et al., 2021], as this is independent of the magnitude of the input signal, and only depends on the frequency, similar to a transfer function. The SIDF of a Clegg Integrator can be represented as $G(\omega)$

$$\begin{aligned}
 G(\omega) &= C(j\omega I - A)^{-1} (I + j\Theta_D(\omega)) B + D \\
 \text{with } \Theta_D(\omega) &= -\frac{2\omega^2}{\pi} \Delta(\omega) [\Gamma_r(\omega) - \Lambda^{-1}(\omega)] \\
 \Lambda(\omega) &= \omega^2 I + A^2 \\
 \Delta(\omega) &= I + e^{\frac{\pi}{\omega} A} \\
 \Delta_r(\omega) &= I + A_r e^{\frac{\pi}{\omega} A} \\
 \Gamma_r(\omega) &= \Delta_r^{-1}(\omega) A_r \Delta(\omega) \Lambda^{-1}(\omega)
 \end{aligned} \tag{2.17}$$

where $A B C D$ are the state space matrices of the reset element. The DF of a Clegg Integrator in frequency domain is shown in Figure 2.15. It is clear that the magnitude closely resembles the characteristics of a linear integrator, but the phase has a lead of 52° as compared to the linear case. This effect is due to the reset action, and is a clear violation of Bode's gain-phase relationship. Researchers have used this to obtain higher bandwidths and better time domain characteristics [Guo et al., 2015].

It should be noted that although SIDFs produce a sinusoidal output, this is just an approximation. The output of a Clegg Integrator contains jumps, resulting in sharp edges. These sharp edges cannot be accurately captured with a single harmonic. When examining the describing function of the Clegg integrator to a sinusoidal input, the describing

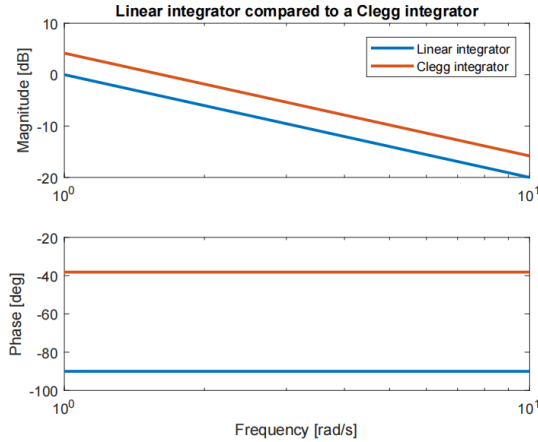


Figure 2.15: Describing Function of a Clegg Integrator compared to a Linear Integrator

function suggests that the output is a sine wave with a phase shift of -38° . However, the output is very different as seen in Figure 2.16. This is essential to keep in mind while designing reset filters that, DFs can only be used as a primary tool and only a time-domain simulation or experiments can give insights of how the system would really behave.

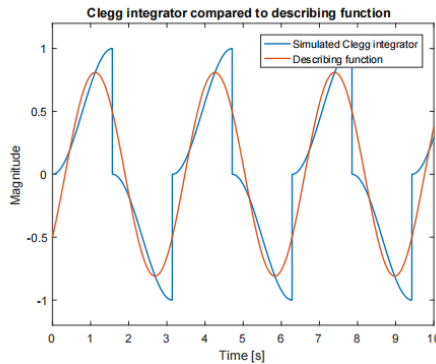


Figure 2.16: Actual output compared to a describing function output of the Clegg integrator

HIGHER ORDER SINUSOIDAL INPUT DFs (HOSIDFs)

Nonlinear systems when subjected to a single input generates multiple harmonics, in contrast to a linear system. The SIDF described earlier is just the fundamental or first harmonic of the output of a reset system. Higher order harmonics are also generated and these are termed as Higher Order Sinusoidal Input Describing Functions (HOSIDFs), as mentioned in [Nuij et al., 2006]. The nonlinear system can be visualized as a virtual harmonic generator as shown in Figure 2.17. When a sine wave of frequency ω is inserted, the virtual harmonic generator generates harmonics of frequencies $\omega, 2\omega, 3\omega, \dots$,

$n\omega$. These harmonics are inserted in several describing functions denoted with $H_n(\omega)$ in Figure 2.17. The even harmonics are zero for reset systems.

This means the DF representation in frequency domain of a reset system can be extended by including HOSIDFs as $G(\omega, n)$, where n denotes the n^{th} harmonic

$$G(\omega, n) = \begin{cases} C(j\omega I - A)^{-1} (I + j\Theta_D(\omega)) B + D & \text{for } n = 1 \\ C(j\omega n I - A)^{-1} j\Theta_D(\omega) B & \text{for odd } n \geq 2 \\ 0 & \text{for even } n \geq 2 \\ \text{with } \Theta_D(\omega) & = -\frac{2\omega^2}{\pi} \Delta(\omega) [\Gamma_r(\omega) - \Lambda^{-1}(\omega)] \\ \Lambda(\omega) & = \omega^2 I + A^2 \\ \Delta(\omega) & = I + e^{\frac{\pi}{\omega} A} \\ \Delta_r(\omega) & = I + A_r e^{\frac{\pi}{\omega} A} \\ \Gamma_r(\omega) & = \Delta_r^{-1}(\omega) A_r \Delta(\omega) \Lambda^{-1}(\omega) \end{cases} \quad (2.18)$$

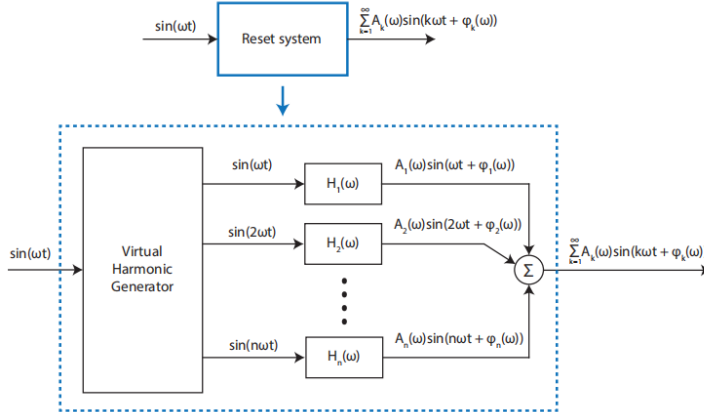


Figure 2.17: Virtual harmonics generator and higher order DFs of a reset system

These higher order harmonics can considerably affect the performance of a reset control system by introducing high frequency dynamics and excessive control action. It can also affect the loop-shaping design process that is usually adopted to design reset control systems in frequency-domain, if the relative magnitudes of HOSIDFs are comparable or greater than the magnitudes of the first harmonic. Several strategies have been adopted to tackle this issue such as bandpassing non-linearities in a certain frequency band [Karbasizadeh et al., 2020], optimization based design of reset control to suppress higher order harmonics [Saikumar et al., 2021].

FIRST ORDER RESET ELEMENT (FORE)

The First Order Reset Element (FORE) was introduced by [HOROWITZ and ROSENBAUM†, 1975] as a generalization of the Clegg Integrator. A FORE can be considered as a reset version of a first order low-pass filter, in the frequency domain. In state-space form, a state

matrix A is added to the continuous-time dynamics, in addition to the input matrix. This is represented as

$$\begin{cases} \dot{x}_c = -\omega x_c(t) + \omega e(t), & \text{when } e(t) \neq 0 \\ x_c^+ = 0, & \text{when } e(t) = 0 \\ y(t) = x_c(t) \end{cases} \quad (2.19)$$

where ω is the corner frequency for the low-pass action. In the frequency-domain, the DF and HOSIDFs of a FORE can be represented as shown in Figure 2.18. Here we see that the magnitude characteristics of the first harmonic closely resembles that of a linear low-pass filter, but the phase lag at high frequencies is only -38° . This phase has been used to obtain higher bandwidths for servo systems [Guo et al., 2009]. Since the magnitude of HOSIDFs are lower compared to the first harmonic for a FORE, the DF of a FORE serves as a good analytical tool for loop-shaping-like controller design techniques.

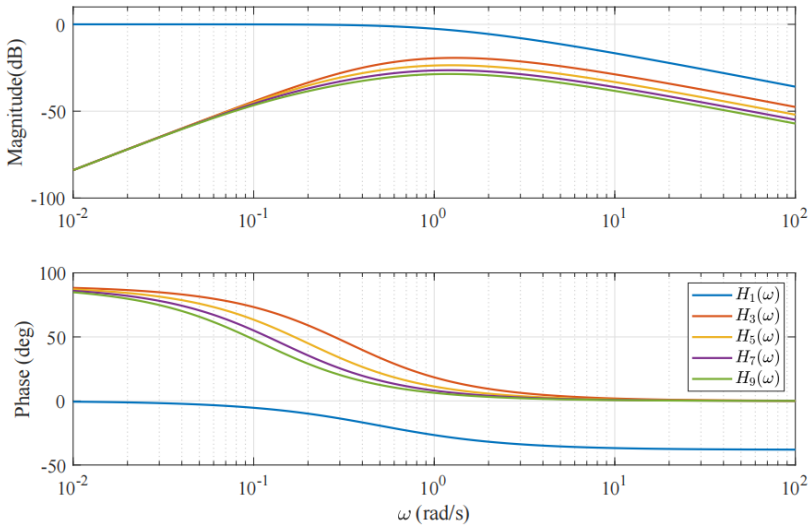


Figure 2.18: Describing functions and HOSIDFs of a FORE

BIBLIOGRAPHY

- Astolfi, A., Nesic, D., & Teel, A. R. (2008). Trends in nonlinear control. *2008 47th IEEE Conference on Decision and Control*, 1870–1882. <https://doi.org/10.1109/CDC.2008.4739513>
- Balas, M. J. (1979). Direct velocity feedback control of large space structures. *Journal of Guidance and Control*, 2(3), 252–253. <https://doi.org/10.2514/3.55869>
- Bupp, R., Bernstein, D., Chellaboina, V., & Haddad, W. (1996). Finite settling time control of the double integrator using a virtual trap-door absorber. *Proceeding of the 1996 IEEE International Conference on Control Applications IEEE International Conference on Control Applications held together with IEEE International Symposium on Intelligent Control*, 179–184.
- Bupp, R. T., Bernstein, D. S., Chellaboina, V. S., & Haddad, W. M. (2000). Resetting virtual absorbers for vibration control. *Journal of Vibration and Control*, 6(1), 61–83. <https://doi.org/10.1177/107754630000600104>
- Cazzulani, G., Resta, F., Ripamonti, F., & Zanzi, R. (2012). Negative derivative feedback for vibration control of flexible structures. *Smart Materials Structures - SMART MATER STRUCT*, 21. <https://doi.org/10.1088/0964-1726/21/7/075024>
- Clegg, J. C. (1958). A nonlinear integrator for servomechanisms. *Transactions of the American Institute of Electrical Engineers, Part II: Applications and Industry*, 77(1), 41–42. <https://doi.org/10.1109/TAI.1958.6367399>
- Creasy, M. A., Leo, D., & Farinholt, K. (2008). Adaptive collocated feedback for noise absorption in payload fairings. *Journal of Spacecraft and Rockets*, 45, 592–599.
- Deenen, D., Heertjes, M., Heemels, W., & Nijmeijer, H. (2017). Hybrid integrator design for enhanced tracking in motion control. *2017 American Control Conference (ACC)*, 2863–2868. <https://doi.org/10.23919/ACC.2017.7963385>
- Fanson, J., & Caughey, T. (1990). Positive position feedback control for large space structures. *AIAA Journal*, 28, 717–724.
- Feuer, A., Goodwin, G., & Salgado, M. (1997). Potential benefits of hybrid control for linear time invariant plants. *Proceedings of the 1997 American Control Conference (Cat. No.97CH36041)*, 5, 2790–2794 vol.5. <https://doi.org/10.1109/ACC.1997.611964>
- GOH, C. J., & CAUGHEY, T. K. (1985). On the stability problem caused by finite actuator dynamics in the collocated control of large space structures. *International Journal of Control*, 41(3), 787–802. <https://doi.org/10.1080/0020718508961163>
- Guo, Y., Wang, Y., & Xie, L. (2009). Frequency-domain properties of reset systems with application in hard-disk-drive systems. *IEEE Transactions on Control Systems Technology*, 17(6), 1446–1453. <https://doi.org/10.1109/TCST.2008.2009066>
- Guo, Y., Xie, L., & Wang, Y. (2015). *Analysis and design of reset control systems*. <https://doi.org/10.1049/PBCE094E>

- Heertjes, M., van den Eijnden, S., Sharif, B., Heemels, M., & Nijmeijer, H. (2019). Hybrid integrator-gain system for active vibration isolation with improved transient response [8th IFAC Symposium on Mechatronic Systems MECHATRONICS 2019]. *IFAC-PapersOnLine*, 52(15), 454–459. <https://doi.org/https://doi.org/10.1016/j.ifacol.2019.11.717>
- Heertjes, M. E., & Vardar, Y. (2013). Self-tuning in sliding mode control of high-precision motion systems [6th IFAC Symposium on Mechatronic Systems]. *IFAC Proceedings Volumes*, 46(5), 13–19. <https://doi.org/https://doi.org/10.3182/201304103-CN-2034.00019>
- Holterman, J. (2002). Vibration control of high-precision machines with active structural elements. *Chemical Engineering Science - CHEM ENG SCI*.
- HOROWITZ, I., & ROSENBAUM†, P. (1975). Non-linear design for cost of feedback reduction in systems with large parameter uncertainty. *International Journal of Control*, 21(6), 977–1001. <https://doi.org/10.1080/00207177508922051>
- Karbasizadeh, N., Dastjerdi, A. A., Saikumar, N., & HosseinNia, S. H. (2020). Band-passing nonlinearity in reset elements.
- Kim, S.-M., & Oh, J.-E. (2013). A modal filter approach to non-collocated vibration control of structures. *Journal of Sound and Vibration*, 332(9), 2207–2221. <https://doi.org/https://doi.org/10.1016/j.jsv.2012.12.002>
- Lin, D., Lan, W., & Li, M. (2011). Composite nonlinear feedback control for linear singular systems with input saturation. *Systems Control Letters*, 60(10), 825–831. <https://doi.org/https://doi.org/10.1016/j.sysconle.2011.06.006>
- Marinangeli, L. (2016). Active vibration control of smart structures using fractional-order control.
- Moheimani, S., & Fleming, A. (2006). Piezoelectric transducers of vibration control and damping.
- Nuij, P., Bosgra, O., & Steinbuch, M. (2006). Higher-order sinusoidal input describing functions for the analysis of non-linear systems with harmonic responses. *Mechanical Systems and Signal Processing*, 20(8), 1883–1904. <https://doi.org/https://doi.org/10.1016/j.ymssp.2005.04.006>
- Preumont, A. (1999). Vibration control of active structures: An introduction. <https://doi.org/10.1023/A:1004398914135>
- Prieur, C., Queinnec, I., Tarbouriech, S., & Zaccarian, L. (2018). Analysis and synthesis of reset control systems. *Foundations and Trends in Systems and Control*, 6, 117–338. <https://doi.org/10.1561/26000000017>
- Saikumar, N., Heinen, K., & HosseinNia, S. H. (2021). Loop-shaping for reset control systems: A higher-order sinusoidal-input describing functions approach. *Control Engineering Practice*, 111, 104808. <https://doi.org/https://doi.org/10.1016/j.conengprac.2021.104808>
- Vidyasagar, M. (1993). *Nonlinear systems analysis (2nd ed.)* Prentice-Hall, Inc.

3

RESEARCH GAP AND OBJECTIVES

In Chapter 2 we covered the existing state-of-art in active damping, and reset control for vibration suppression. We saw that an RVA was able to provide finite-time stabilization for an undamped system. However, even introducing a small amount of damping poses a problem as the plant position never crosses zero when the velocities cross zero (further emphasized in Chapter 4). This means that a reset law based on position feedback no longer works for lightly damped systems. It is also worth mentioning that, if there are parameter uncertainties in the system, the damping performance is affected considerably when using an RVA. Furthermore, the high-pass characteristics of RVAs are not ideal for spillover, if the system to be damped has multiple resonance modes.

In [R. T. Bupp et al., 2000, R. Bupp et al., 1996], RVA design was performed by analytically solving differential equations. Since we have frequency domain techniques at our disposal for reset controller synthesis, it is also natural to consider this approach as a more user-friendly alternative for controller synthesis, especially from an industrial point-of-view.

In [Heertjes et al., 2019], a HIGS bandpass filter was used to improve transient response for active vibration isolation compared to linear techniques. However, this needed high control gains to achieve any conceivable performance advantages over linear controllers. Although the HIGS bandpass filter was designed using describing functions in the frequency-domain, the underlying mechanism by which it provides better transient response, and its relation to the frequency-domain attributes were not fully explored. In [Raimúndez et al., 2011], reset control was used to inject damping by employing an optimal port-Hamiltonian approach. However, this also did not employ frequency-domain techniques to design reset controllers for active damping.

These research gaps illustrate the following problems:

- Linear control techniques do not take transient damping performance into account explicitly. Furthermore, they are limited by Bode's gain-phase relationship and the trajectories have to be continuously differentiable. Hence the levels of transient damping performance they can achieve are limited

- Resetting Virtual Absorbers are not effective for damped plants, and HIGS does not provide a clear understanding of the physics behind how the hybrid action results in better transient damping
- Most nonlinear hybrid damping control methods cannot be designed in the frequency-domain, and this limits its relevance for industries

Hence, the research objectives are formulated as follows:

3

- Develop a reset control strategy for improved transient damping for damped plants. This strategy should provide a clear idea of the underlying principle that results in improved transient damping performance
- Enable the design of such a controller in the frequency-domain and provide rules-of-thumb for quick controller synthesis
- Validate this newly developed active damping strategy on an experimental setup to demonstrate its effectiveness and compare its performance to a linear counterpart
- Explore its sensitivity to tuning parameters and system delays

4

RESETTING VELOCITY FEEDBACK: RESET CONTROL FOR IMPROVED TRANSIENT DAMPING

M.A. Mohan M.B. Kaczmarek S.H. HosseinNia

ABSTRACT *Active vibration control (AVC) is crucial for the structural integrity, precision, and speed of industrial machines. Despite advancements in nonlinear control techniques, most AVC techniques predominantly employ linear feedback control due to their simplicity and ability to be designed in the frequency domain. In this paper we introduce a reset-based nonlinear bandpass filter that uses velocity feedback to improve transient damping of vibrating structures. The approach is motivated from an energy-based mechanistic analysis, which incentivizes the use of reset. A novel feature of our approach is that it works for non-ideal, naturally damped systems, and enables control design in the frequency domain, thus making it industry friendly. We demonstrate the effectiveness of this new filter by numerical simulations and experimental validation on a single degree-of-freedom flexure stage.*

4.1. INTRODUCTION

As the age of digitalization evolves rapidly, there is an ever-increasing demand for improving precision and decreasing production times for industrial automation in general, and semiconductor manufacturing in particular. As these complex machines incorporate flexural elements to overcome friction and backlash, structural vibrations pose a new challenge. These structural resonance modes result in vibrations that reduces the precision, and considerably increase settling times, and thus decreasing the productivity of such devices. Hence, the need for controlling and quickly damping these vibrations is paramount.

4

Active vibration control is a well-studied problem. In most industries, linear control methods are the most dominant. These techniques have the advantages of being easy to analyze and tune, owing to their analysis and design in the frequency-domain. This is particularly advantageous in an industrial setting where loop-shaping methods are preferred. However, these frequency-domain based linear techniques do not explicitly take transient performance into account, which directly relates to settling times. Moreover, nonlinear control techniques hold better promise compared to linear ones, as they are not restricted by Bode's gain-phase relationship, and hence offer better flexibility and trade-offs.

To this end, in [Chen et al., 2002], a nonlinear technique called QMPPF was used to damp forced vibrations, focusing on steady-state damping. In [Olgac and Holm-Hansen, 1995], another nonlinear technique called delayed resonant feedback was used, based on the principle of an electrical realization of a delayed vibration absorber, to absorb the steady-state resonant oscillations. However, both these techniques focus on steady-state damping performance. In addition to this, the frequency-domain analysis tools are rendered ineffective for the latter. Therefore, we require a nonlinear control technique that can be designed in the frequency-domain, thereby increasing its relevance for industries.

Reset control is a nonlinear hybrid control technique that uses jumps in state trajectories to improve transient performance, [Guo et al., 2015] and allow design in the frequency-domain using Describing Functions (DF). In the insightful work in [R. T. Bupp et al., 2000], Resetting Virtual Absorbers (RVAs) were introduced to achieve finite-time vibration attenuation for plants without damping. This analysis was motivated by energy principles and damping injection through reset, thereby providing a clear incentive for the use of reset. However, the effectiveness of this technique reduces with non-zero plant damping. Moreover, the absence of frequency-domain techniques to design RVAs limits their adoption by industries. Hybrid Integrator Gain Switching (HIGS) is another nonlinear hybrid control technique initially introduced in [Deenen et al., 2017]. In [Heertjes et al., 2019], a HIGS bandpass filter was used to improve transient response for active vibration isolation compared to linear techniques. However, this needed high control gains to achieve any conceivable performance advantages over linear controllers. Although the HIGS bandpass filter was designed using describing functions in the frequency-domain,

the underlying mechanism by which it provides better transient response, and its relation to the frequency-domain attributes were not fully explored. In [Raimúndez et al., 2011], reset control was used to inject damping by employing an optimal port-Hamiltonian approach. However, this also did not employ frequency-domain techniques to design reset controllers for active damping.

This begs the question: How can reset control be used to guarantee better transient damping performance for damped systems compared to linear control? Furthermore, how can they be systematically designed in the frequency-domain, to ease tuning, implementation, and adoption by industries?

In this paper, we introduce a novel reset-based bandpass filter that employs velocity feedback to achieve finite-time vibration suppression for damped systems and compare its performance to a linear bandpass filter. We start with the work of [R. Bupp et al., 1996] and adopt a velocity feedback framework to extend its effectiveness to damped plants. Since the original analysis in [R. Bupp et al., 1996] stems from an energy-based mechanistic approach, our technique also provides an understanding of the underlying mechanism for the improved transient response, as opposed to HIGS. Furthermore, owing to the more aggressive nature of reset compared to HIGS, improvement in transient response is possible with lower control gains which makes our method more energy efficient.

We also develop tuning rules based on describing functions to design this filter in the frequency-domain, thereby increasing its relevance for industries. Staying true to this ethos, the stability of the novel bandpass filter and the closed-loop system is proven using passivity arguments, which only require the base linear transfer function of the reset element and the transfer function of the plant.

An important aspect of this work is that it must be easily implementable on systems in the real-world. Here we experimentally demonstrate the effectiveness of the Resetting Velocity Feedback (RVF) framework for transient damping using a single degree-of-freedom flexure stage. While preliminary, our experimental results show great promise and agree with numerical simulations. The results are also easily extendable to distributed parameter systems.

4.2. PRELIMINARIES

To fully appreciate Resetting Velocity Feedback, three key ideas must be understood: (1) Reset control and its analysis in the frequency-domain using describing functions, (2) Negative Derivative Feedback, and (3) the concept of Resetting Virtual Absorbers (RVAs). In this section we introduce these topics independently. Combining ideas from these approaches, we develop the Resetting Velocity Feedback framework in Section 4.3, and analyze its stability properties. Numerical and experimental results of this novel technique follow in Section 4.4. Finally, Section 4.5 summarizes the study and suggests recommendations for future work

4.2.1. RESET CONTROL AND DESCRIBING FUNCTIONS

Reset control systems are a class of hybrid dynamical systems. In this study we are concerned with zero-crossing reset systems with the general dynamics given by:

$$\begin{aligned} \dot{x}(t) &= Ax(t) + Bu(t) & u(t) &\neq 0 \\ x(t^+) &= A_r x(t) & u(t) &= 0 \\ y(t) &= Cx(t) + Du(t) \end{aligned} \tag{4.1}$$

where the matrices $A, B, C,$ and D describe the state-space matrices of the reset element, $u(t)$ is the error input, $x(t)$ are the states, and $y(t)$ is the controller output. The linear dynamics given by the first and third equations of Equation 4.1 are referred to as the base linear system. The controller states propagate according to the base linear system if the input $u(t) \neq 0$. Whenever the reset conditions are met, i.e., $u(t) = 0$, specified controller states are reset according to the reset matrix A_r . Several sets of reset conditions are presented in literature. Dominant reset conditions in literature are either based on zero-crossings of the error [Beker et al., 2004], based on the signs of the reset controller states and plant output [Nešić et al., 2008], or reset at fixed time instants. This work focusses on reset elements based on zero-crossings of the error with full reset ($A_r = 0$), as they are the most widely studied, applied, and tested [Saikumar et al., 2019].

RESET ELEMENTS

Clegg Integrator (CI): This was the first reset element, introduced by Clegg in 1958 [Clegg, 1958]. The time-domain response of such an integrator is shown in Figure 4.1. As can be seen, the output of the CI resets to zero, whenever the input crosses zero. At all other instances, it follows a similar trajectory as a linear integrator, according to its base linear system dynamics. The state-space matrices of a CI are:

$$A = 0; \quad B = 1; \quad C = 1; \quad D = 0; \quad A_r = 0$$

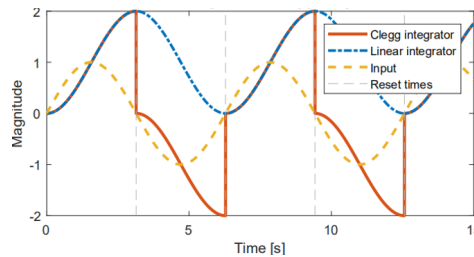


Figure 4.1: Response of a CI and a linear integrator to a sinusoidal input, showing zero-crossing reset actions

First Order Reset Element (FORE): CI was extended to a First Order Reset Element in [HOROWITZ and ROSENBAUM†, 1975]. FORE provides the advantage of filter frequency placement unlike CI, and has been used for narrow-band phase compensation in [Guo et al., 2009]. The FORE’s base linear system is a linear first-order low-pass filter. The state-space matrices of a FORE where the base linear low-pass filter has corner frequency ω_r are:

$$A = -\omega_r; \quad B = \omega_r; \quad C = 1; \quad D = 0; \quad A_r = 0$$

DESCRIBING FUNCTIONS

Describing Functions (DF) are a quasi-linearization of a nonlinear element subject to certain excitation input used to approximately analyze the behaviour of nonlinear systems. DF is a powerful tool for investigating behaviours of elements with hard nonlinearities including dead zone, backlash, and hysteresis, and has been applied in limit cycle predictions and control design [Vidyasagar, 1993]. Furthermore, DFs allow us to analyze reset systems in frequency domain and apply loop-shaping like techniques for control design, which is the de-facto standard in industries [Saikumar et al., 2021].

The Sinusoidal Input DF (SIDF), which uses sinusoidal inputs as excitation signals, is the most widely used describing function technique to analyze reset systems [Guo et al., 2009, Saikumar et al., 2021]. The SIDF of a reset element can be represented as $G(j\omega)$ as introduced in [Guo et al., 2009]

$$\begin{aligned}
 G(\omega) &= C(j\omega I - A)^{-1} (I + j\Theta_D(\omega)) B + D \\
 \text{with } \Theta_D(\omega) &= -\frac{2\omega^2}{\pi} \Delta(\omega) [\Gamma_r(\omega) - \Lambda^{-1}(\omega)] \\
 \Lambda(\omega) &= \omega^2 I + A^2 \\
 \Delta(\omega) &= I + e^{\frac{\pi}{\omega} A} \\
 \Delta_r(\omega) &= I + A_r e^{\frac{\pi}{\omega} A} \\
 \Gamma_r(\omega) &= \Delta_r^{-1}(\omega) A_r \Delta(\omega) \Lambda^{-1}(\omega)
 \end{aligned} \tag{4.2}$$

where A, B, C, D are the state-space matrices of the reset element. Although reset systems are nonlinear, DFs only depend on the frequency of the input signal and not on the magnitude, unlike certain other nonlinear systems. This makes them an ideal candidate for frequency-domain analysis. The DF of a FORE in the frequency-domain is shown in Figure 4.2. The magnitude closely resembles the characteristics of a linear low-pass filter, but the phase lag is limited to -38° . In this paper we will use FOREs and its DF to implement the Resetting Velocity Feedback framework.

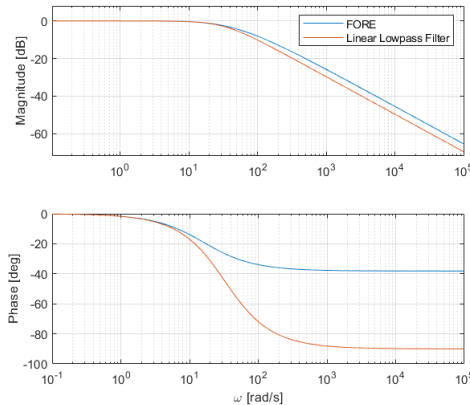


Figure 4.2: Describing function of a FORE compared to an FRF of a linear low-pass filter

4.2.2. NEGATIVE DERIVATIVE FEEDBACK

Direct Velocity Feedback (DVF) is a well understood active damping technique in which structural (modal) velocity is negatively feedback to impart damping [Balas, 1979]. In [Cazzulani et al., 2012], this study was extended by feeding back velocity through a band-pass filter tuned to the eigenfrequency of the mode to eliminate low- and high-frequency spillover. This is termed as Negative Derivative Feedback (NDF) and is represented schematically in Figure 4.3.

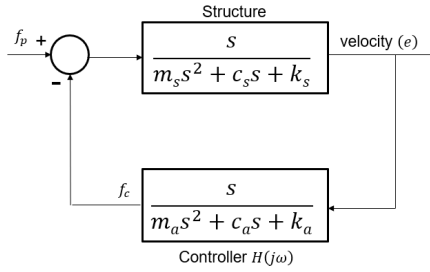


Figure 4.3: Block diagram representation of NDF for a single DOF oscillator

For such a system, a physical analogy can be drawn as pointed out by [Kim and Oh, 2013], and as shown in Figure 4.4. The closed-loop negative feedback interconnection in Figure 4.3 represents an oscillator-vibration absorber setup, where the controller performs the role of an emulated dynamic vibration absorber. This physical analogy also holds true for a negative position feedback framework [Kim and Oh, 2013]. This mechanical analogy will be exploited later on in Section 3 to develop RVF and prove stability.

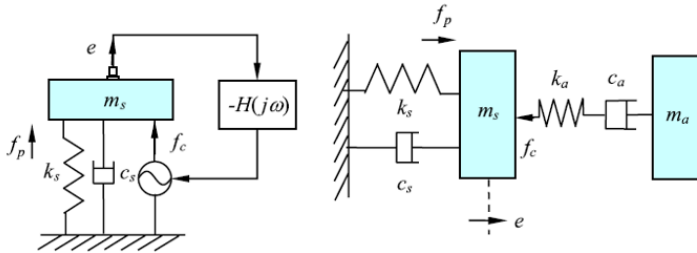


Figure 4.4: Physical analogy of the NDF framework [Kim and Oh, 2013]

4.2.3. RESETTING VIRTUAL ABSORBERS

The concept of a resetting virtual absorber is based on the insightful analysis found in [R. T. Bupp et al., 2000, R. Bupp et al., 1996]. which shows how reset can inject damping into an undamped system consisting of a single degree-of-freedom oscillator and an emulated vibration absorber, for finite-time vibration suppression.

Consider a single degree-of-freedom undamped oscillator with mass M and stiffness K , in series with an emulated dynamic vibration absorber with mass m and stiffness k , whose states (position and velocity), can be instantaneously reset to zero. This is shown

in Figure 4.5. According to the physical analogy of vibration controllers introduced earlier in Section 4.2.2, this emulated vibration absorber can be considered an active damping controller, which uses the position of mass M as its input. As a block diagram, this can be represented as shown in Figure 4.6 (the diagonal arrow denotes a reset element).

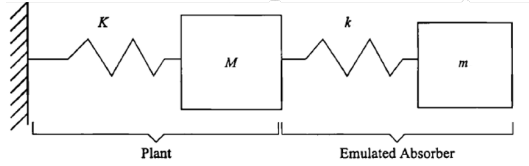


Figure 4.5: The model of a Resetting Virtual Absorber [R. Bupp et al., 1996]

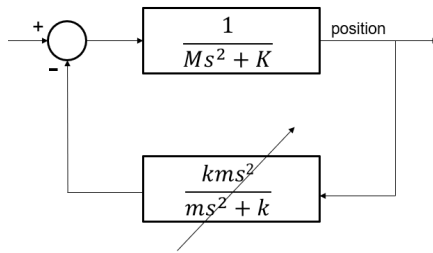


Figure 4.6: Block diagram representation of the RVA framework

For an impulse excitation to mass M , for $m = 1.33M$ and $k = 1.33K$ [R. Bupp et al., 1996], the response of the system is shown in Figure 4.7. When the position of mass M reaches zero for the first time, the velocities of masses M and m are also simultaneously zero, as indicated in Figure 4.7. Therefore, the energy contained in the system at this instant is uniquely due to the compression of spring k , i.e., the non-zero position of mass m . In other words, all the energy is contained within the emulated absorber.

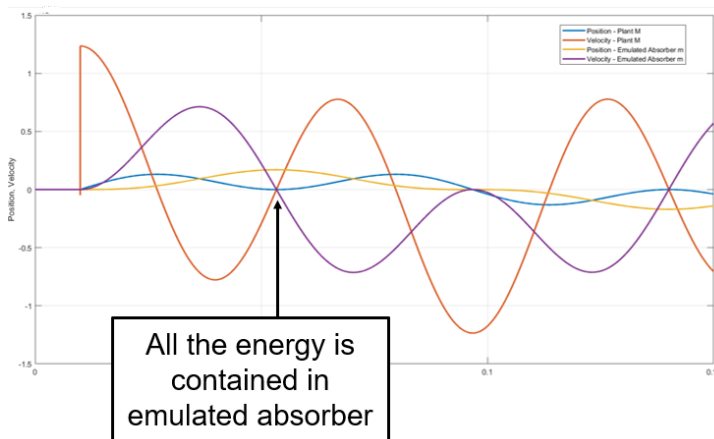


Figure 4.7: Response of the system in Figure 4.5 to an impulse excitation on mass M

If the states (virtual position and velocity) of the emulated absorber (controller) are reset to zero at this exact instant, the total energy in the system is instantaneously dissipated before it redistributes it to the states of mass M . Hence, damping is injected into the system by resetting the states of the controller. This results in finite-time suppression of the oscillations of mass M , as shown in Figure 4.8. Reset is the only source for damping as this system has no natural damping whatsoever. The control effort is the force provided by the compression of spring k and can be seen to follow a smooth trajectory until the point where the position of mass M hits zero. It is then instantaneously reset to zero as shown in Figure 4.8.

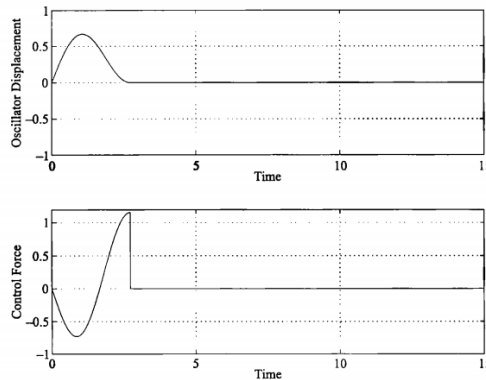


Figure 4.8: Finite-time vibration suppression using RVA [R. Bupp et al., 1996]

4.3. FRAMEWORK

In this section, the three independent concepts introduced in Section 4.2 are combined to develop the Resetting Velocity Feedback (RVF) framework. The stability properties of the novel reset controller and the closed-loop system are also analysed using a passivity-based approach.

4.3.1. FROM RVA TO RVF

As seen earlier, RVAs are based on position feedback of undamped plants, designed to reset when plant position hits zero. However, therein lies the problem: For damped plants, the plant position no longer hits zero at the desired point, but remains ever so slightly positive, as shown in Figure 4.9. Even though this time instant corresponds to a point of minimum plant and maximum controller energy, the zero position-based reset law no longer holds. Fortunately, the plant velocity does cross zero at this point (of minimum plant energy) and thus motivates the use of a reset law based on velocity feedback. This ensures the reset of controller states when the controller has maximum energy, thereby taking away most of the energy in the system and injecting damping.

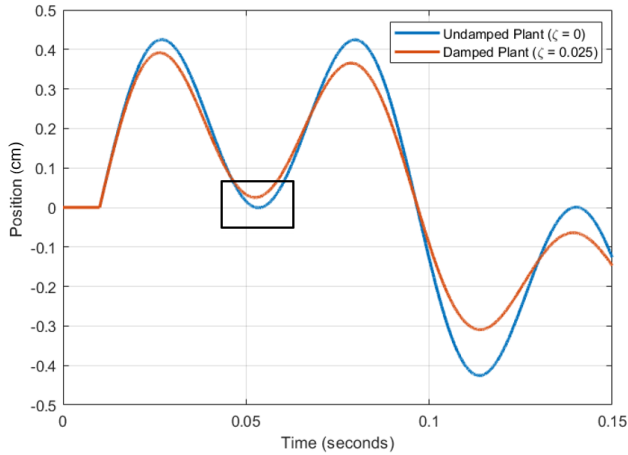


Figure 4.9: Position trajectories for damped and undamped plants showing the ineffectiveness of zero-crossing position feedback. The point-of-interest is highlighted with a rectangular box

Our feedback framework needs to be slightly modified to account for velocity feedback compared to Figure 4.6, as shown in Figure 4.10. This framework resembles the NDF system presented earlier, with the linear bandpass controller being replaced by a reset alternative. A damping term is also added (with the same damping ratio as the plant) to match the resonance frequency of the emulated absorber to that of the plant.

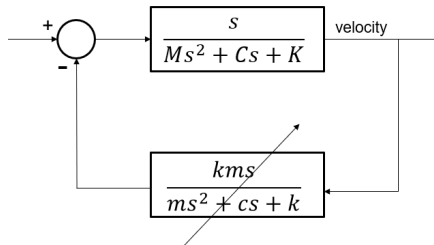


Figure 4.10: Modified block diagram to account for velocity feedback which also includes a damping term in the controller structure

As the main aim of our work is to systematically design reset controllers in frequency domain, we analyze this “new” reset filter in frequency domain using its describing function. This is shown in Figure 4.11. Two aspects are worth noting: (1) At the resonance frequency of the controller $\omega_c = 65 \text{ rad/s}$, the describing function has a gain of 31.9, which corresponds to a dimensionless active damping ratio $\zeta_{active} = \frac{km}{2\sqrt{KM}} = 0.55$ and (2) a phase of about -19.09° (different from a linear bandpass filter which has a phase of 0° at its resonance frequency). The phase becomes slightly less negative with increased damping. As long as the $\frac{k}{m}$ ratio is maintained, changing m and k does not affect the phase characteristics, but only adds a constant gain.

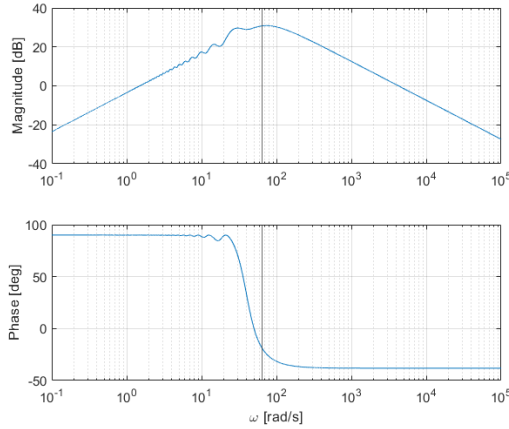


Figure 4.11: Describing function of the reset element in Figure 4.10. The vertical line highlights the target frequency

Although this reset filter appears promising from describing function analysis, reset systems with second-order bandpass structures are not well-studied. Reset systems are also unique in the sense that, for the same base linear system, different state-space realizations result in different closed-loop behaviour. Hence, our aim is to “emulate” the ζ_{active} and phase of this describing function at ω_c , with a reset bandpass filter built from commonly-used and well-understood reset elements. This is obtained by subtracting a FORE with corner frequency ω_1 from a FORE with corner frequency ω_2 , with $\omega_2 > \omega_1$. Since FOREs have a unique state-space realization, this approach eliminates ambiguities on which state-space realization to implement. The well-studied nature of FOREs in the reset control community also makes the choice of using them straight-forward. These are tuned to the appropriate gain and phase value at ω_c . The resulting FORE-based bandpass filter for active damping can be represented as

$$R_{bp} = g(FORE_{\omega_2} - FORE_{\omega_1}) \tag{4.3}$$

where g is the gain required to ensure $\zeta_{active} = 0.55$. The structure is shown schematically in Figure 4.12. The corner frequencies of the FOREs are obtained by solving an optimization problem involving the phase of the describing function of R_{bp} , formulated as:

$$\operatorname{argmin}_{\omega_1, \omega_2} |\angle R_{bp} - 19.09^\circ|$$

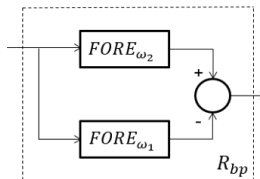


Figure 4.12: Structure of R_{bp}

The describing function of this novel FORE-based bandpass filter is shown in Figure 4.13 and compared to the second-order bandpass filter introduced earlier. Clearly, the magnitude and phase at the plant eigenfrequency $\sqrt{K/M} = 65 \text{ rad/s}$, are equal. Furthermore, the slope of the phase characteristics of this FORE-based bandpass filter is lower at $\omega = \sqrt{K/M}$. This results in better robustness to plant uncertainties.

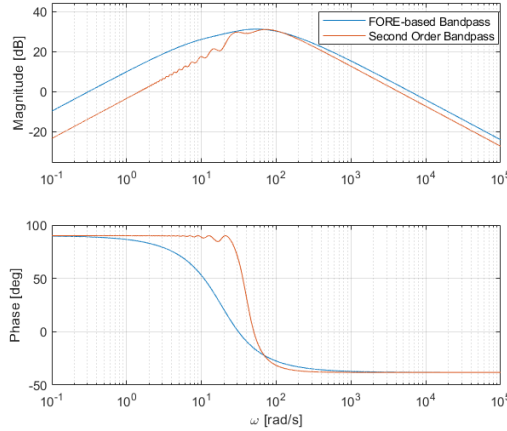


Figure 4.13: Describing function of a FORE-based bandpass filter compared to the second-order bandpass filter. Both provide the same magnitude and phase values at the target frequency of 65 rad/s

For easy implementation in practice, the following rules-of-thumb are nearly optimal for plants with 1%-2% natural damping:

- Choose $\omega_1 = 0.4\sqrt{K/M}$ and $\omega_2 = 0.75\sqrt{K/M}$. This ensures a phase of -19.09° at the target frequency
- Choose gain g , such that the magnitude of the describing function of R_{bp} , $|R_{bp}|_{\omega=\sqrt{K/M}} = (2) \cdot (0.55) \cdot \sqrt{KM}$, provided the plant transfer function is of the form as shown in Figure 4.14. This ensures that the dimensionless active damping ratio, $\zeta_{active} = 0.55$, at the target frequency.

Once the parameters have been calculated, the gain value can be fine-tuned to achieve optimal transient damping performance. The closed-loop system with such a FORE-based bandpass filter and a damped single degree-of-freedom plant constitutes the Resetting Velocity Feedback (RVF) framework, as shown in Figure 4.14. The framework is summarized schematically in Figure 4.15.

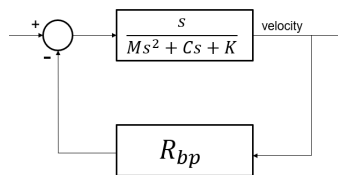


Figure 4.14: Resetting Velocity Feedback (RVF) framework

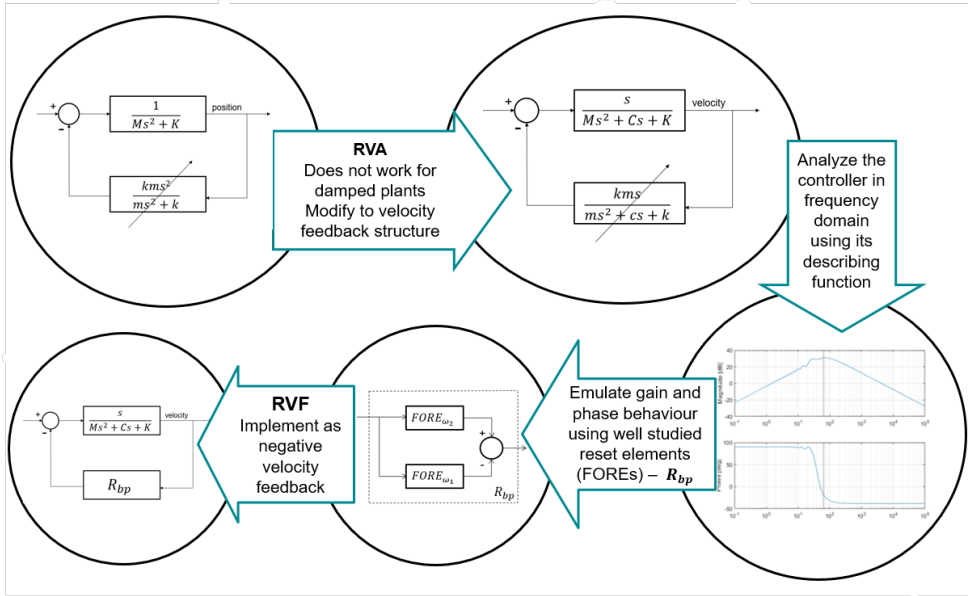


Figure 4.15: Development of the Resetting Velocity Feedback framework at a glance

4.3.2. STABILITY ANALYSIS

We now address the stability properties of (1) the reset bandpass filter R_{bp} and, (2) the closed-loop system of RVF. The following three theorems on passivity will serve as a baseline for this analysis:

Theorem 1: [Carrasco et al., 2010] For an LTI system with transfer function $H(s) = C(sI - A)^{-1}B + D$, with A Hurwitz and the pair (A, B) controllable, it holds that: The system is passive if and only if $Re(H(j\omega)) \geq 0$ for all ω . The system is Output Strictly Passive (OSP) if and only if there is an ϵ such that $Re[H(j\omega)] \geq \epsilon |H(j\omega)|^2$ for all ω

Theorem 2: [Carrasco et al., 2010] A full reset compensator R is passive, ISP, OSP, or VSP if the base compensator is passive, ISP, OSP, or VSP, respectively.

Corollary 1: In our case, the reset bandpass filter R_{bp} is formed by two FOREs in parallel with corner frequencies ω_1 and ω_2 with $\omega_2 > \omega_1 > 0$, resulting in the following base linear transfer function:

$$R_{bp}(j\omega) = \frac{(\omega_2 - \omega_1)j\omega}{(j\omega + \omega_1)(j\omega + \omega_2)} \quad (4.4)$$

$$Re[R_{bp}(j\omega)] = \frac{\omega^2(\omega_2 - \omega_1)(\omega_2 + \omega_1)}{(\omega_1\omega_2 - \omega^2)^2 + (\omega_1 + \omega_2)^2\omega^2} \quad (4.5)$$

$$|R_{bp}(j\omega)|^2 = \frac{\omega^2 (\omega_2 - \omega_1) (\omega_2 + \omega_1)}{(\omega_1 \omega_2 - \omega^2)^2 + (\omega_1 + \omega_2)^2 \omega^2} \quad (4.6)$$

Clearly, $\text{Re}[R_{bp}(j\omega)] \geq 0$ for all ω , and $\text{Re}[R_{bp}(j\omega)] \geq c |R_{bp}(j\omega)|^2$ for $c = 1$. Hence, according to Theorem 1 and Theorem 2, the reset-based bandpass filter is OSP.

Similarly, it can be shown that the plant, with the transfer function from force to velocity, is also OSP, as its transfer function also has a similar structure.

Theorem 3: [Carrasco et al., 2010] The negative feedback interconnection between an LTI plant P and a full reset compensator R , with base linear compensator R_{bl} , is finite-gain stable if one of the following conditions are satisfied:

- R_{bl} is ISP, and P is ISP
- R_{bl} is OSP, and P is OSP
- R_{bl} is VSP, and P is passive
- R_{bl} is passive, and P is VSP

Corollary 2: From Corollary 1 and Theorem 3, we can assert that the negative feedback interconnection of the reset-based bandpass filter and the plant with velocity output is finite-gain stable, as they are both OSP. Hence the Resetting Velocity Feedback framework is finite-gain stable.

4.4. RESULTS

While describing functions simplify the analysis of reset systems, they are still only approximations of the actual system. Empirical evidence is needed to determine whether the framework developed earlier holds true in practice. In this section we report evidence on the previously developed Resetting Velocity Feedback structure, through numerical simulations and experimental testing.

To focus on controller validation, the physical system is chosen to be a simple single degree-of-freedom flexure stage. A Lorentz actuator (ETEL 025C) is used to provide both, the disturbance signal and the control force. A Polytec OFV-505 Laser Doppler Vibrometer (LDV) is used as a velocity sensor, which provides voltage signals proportional to the vibration velocity. National Instruments compactRIO FPGA is used to acquire the signals, and compute and deliver the control signal to the current-source power amplifier. LabVIEW 2020 is used to interface the host computer with compactRIO. The experimental setup is shown in Figure 4.16.

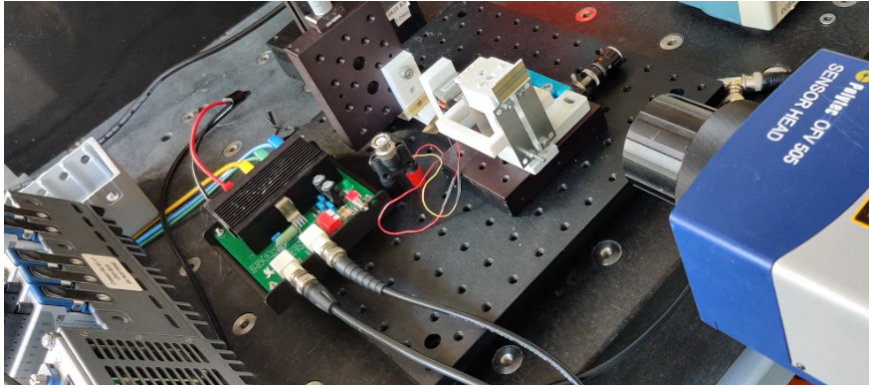


Figure 4.16: Experimental setup

4

System identification is performed by exciting the system with a chirp (swept sine) signal. Using MATLAB's System Identification Toolbox, the Frequency Response Function (FRF) of the system is obtained, as shown in Figure 4.17. As expected, this denotes the transfer function from force to velocity, and is a reasonable estimate of a single degree-of-freedom lumped-mass model, with an eigenfrequency at 13.2 Hz. A transfer function is fitted to the experimental data using MATLAB's `tfestimate` function, and is given by Equation 4.7

$$P(s) = \frac{555.2s}{s^2 + 2.882s + 6972} \tag{4.7}$$

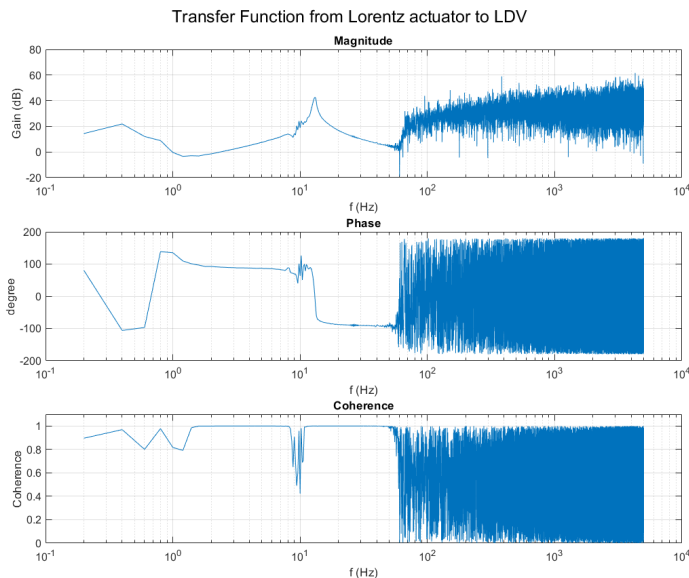


Figure 4.17: FRF of the experimentally identified system

With the plant parameters identified experimentally, the method described in Section 4.3 is followed to obtain the reset bandpass filter, R_{bp} . For the plant $P(s)$, the R_{bp} parameters are: $\omega_1 = 33.4$ rad/s, $\omega_2 = 62.62$ rad/s and $g = 0.875$.

For experiments, the sampling frequency is chosen to be 10 kHz. This is significantly higher than the eigenfrequency to avoid aliasing, but well within the limits of the FPGA's computational capabilities. Before deploying the discrete controller on the experimental setup, it is numerically simulated using MATLAB/Simulink. A pulse disturbance is imparted to the system revealing its transient damping performance. For a comparative study, a linear bandpass filter L_{bp} is designed with its transfer function given by Equation 4.8

$$L_{bp}(s) = \frac{36s}{(s + 167)(s + 41.75)} \quad (4.8)$$

This linear bandpass filter is designed to have the same gain as R_{bp} , and 0° of phase, at the plant's eigenfrequency of 13.2 Hz. The equal gain value of both filters ensure a similar peak control force and is a practical measure to compare control performance. The describing function of R_{bp} and the FRF of L_{bp} is shown in Figure 4.18. Figure 4.19 shows the simulation results for the pulse disturbance. The reset-based bandpass filter (RVF) provides a 220.3% improvement in settling time compared to the linear bandpass filter (NDF).

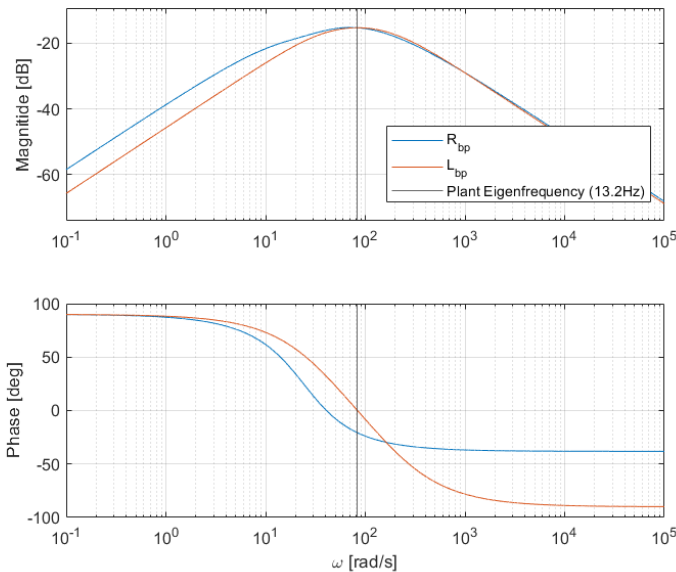


Figure 4.18: Describing function of R_{bp} compared to the FRF of L_{bp} . Both are tuned to provide the same gain at 13.2 Hz

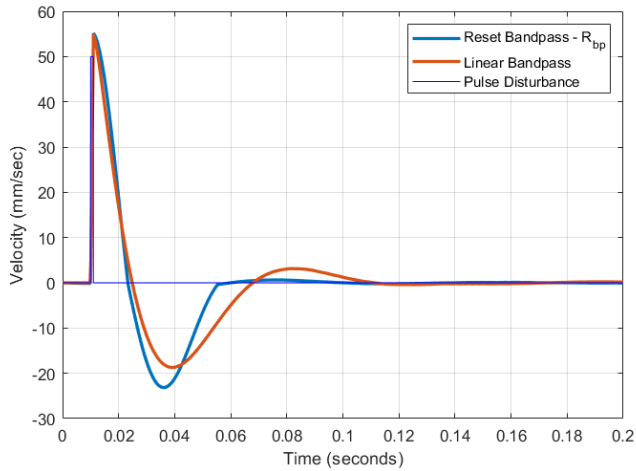


Figure 4.19: Comparison of system responses to a pulse disturbance (simulation)

For the experimental study, a finite-time sinusoidal excitation at 13.2 Hz is applied for 2708 ms (36 complete cycles). This is done as a finite-time sinusoidal disturbance reveals both steady-state and transient damping performance. These results are shown in Figure 4.20, with the emphasis placed on transient response. The experimental results are representative of the numerical simulations. RVF provides a 273.1% increase in settling time compared to NDF, for the same control gain. The steady-state damping performance of RVF is marginally worse compared to NDF. This is to be expected as the focus of RVF design was to ensure better transient performance.

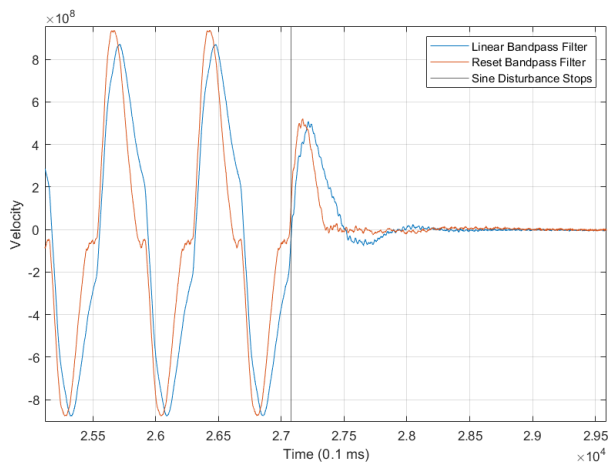


Figure 4.20: Comparison of system responses to a finite sinusoidal excitation (experiment)

4.4.1. SENSITIVITY ANALYSIS

Reset systems are much more sensitive to tuning than conventional linear systems. Therefore, it is important to quantify its sensitivity to tuning parameters (control gain) experimentally. We see that for a 10% variation in control gain, the transient performance is still superior to the nominal linear bandpass filter. The results are shown in Figure 4.21 and summarized in Table 4.1. These results illustrate that even though the reset bandpass filter is not explicitly designed to be robust, it still shows relatively low sensitivity to tuning parameters.

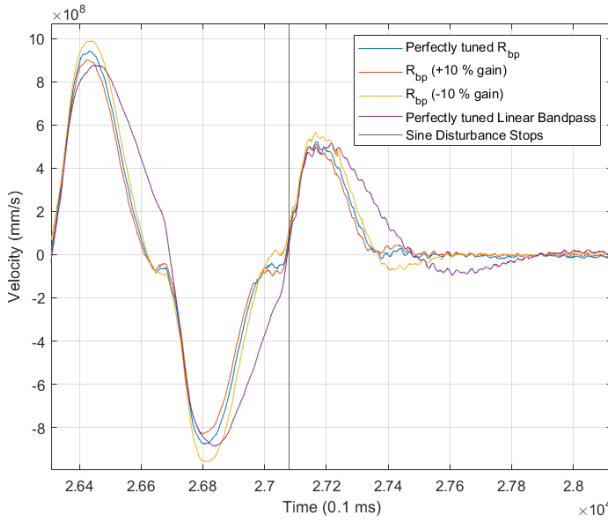


Figure 4.21: Sensitivities of transient damping performance to gain variation

Controller	Settling Time	Deterioration w.r.t nominal R_{bp}
R_{bp} (+10% gain)	41 ms	29.9%
R_{bp} (-10% gain)	53 ms	69.8%
Nominal L_{bp}	82 ms	273.1%

Table 4.1: Sensitivity of settling times to control gain

As far as (known) system delays are concerned, the reset bandpass filter can be tuned to provide a certain phase at the plant eigenfrequency such that the net phase including the delay amounts to about -19.09° . This further emphasizes the flexibility offered by using two independent FOREs, as it is possible to manipulate the phase characteristics without considerably changing the magnitude characteristics. This would be not possible for a linear bandpass filter. For a delay of 2 milliseconds (amounting to -10° of phase lag at the target frequency), the simulation results for a pulse disturbance, of a re-tuned reset bandpass filter with delay compensation is compared to a reset bandpass without delay compensation in Figure 4.22. The control gain is kept constant as the nominal case without system delays. The bandpass filter with delay compensation performs similar to

a system without delays. This illustrates that reset can also be used to actively compensate for known time-delays.

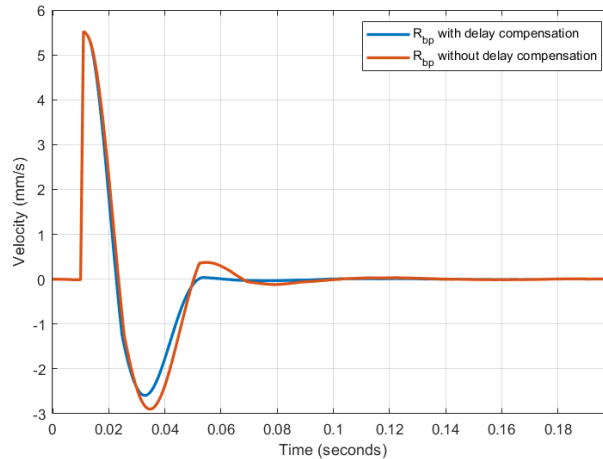


Figure 4.22: RVF performance for systems with known time-delays

4.5. CONCLUSIONS AND FUTURE WORK

This paper presented our efforts at using reset control to achieve improved transient damping compared to linear control methods. The approach is motivated by an energy-based mechanistic analysis of the base linear systems, which provides clear insight for the use of reset in such problems. Translating these insights into the frequency-domain using describing functions and rules-of-thumb for systematic control design, greatly simplifies the application of reset control for vibration control problems and makes it relevant for industrial applications. The numerical and experimental results validate the approach and demonstrate its superiority compared linear to methods such as NDF, by providing a 273.1% increase in settling time for the same control gain. We also empirically showed that this novel reset-based bandpass filter is robust with respect to tuning parameters and can also compensate for known system delays.

As future work, the study can be extended to more complex distributed parameter systems. Multiple (and non-collocated) modes may render the plant non-passive and affect stability. This could be a direction for future research. Presently, the controller is not explicitly designed to be robust to plant variations. An adaptive scheme can be incorporated into this framework to improve its performance in uncertain environments. The design of a robust version of the controller could also be explored. Although the analysis is motivated from energy principles and describing functions, a rigorous mathematical treatment on how the reset bandpass filter provides better transient response is yet to be performed. Finally, a theoretical treatment on the effect of delays on system performance is also left out. Further theoretical questions remain unanswered in these directions and could pave the way for interesting future research.

BIBLIOGRAPHY

- Balas, M. J. (1979). Direct velocity feedback control of large space structures. *Journal of Guidance and Control*, 2(3), 252–253. <https://doi.org/10.2514/3.55869>
- Beker, O., Hollot, C., Chait, Y., & Han, H. (2004). Fundamental properties of reset control systems. *Automatica*, 40(6), 905–915. <https://doi.org/https://doi.org/10.1016/j.automatica.2004.01.004>
- Bupp, R., Bernstein, D., Chellaboina, V., & Haddad, W. (1996). Finite settling time control of the double integrator using a virtual trap-door absorber. *Proceeding of the 1996 IEEE International Conference on Control Applications IEEE International Conference on Control Applications held together with IEEE International Symposium on Intelligent Control*, 179–184.
- Bupp, R. T., Bernstein, D. S., Chellaboina, V. S., & Haddad, W. M. (2000). Resetting virtual absorbers for vibration control. *Journal of Vibration and Control*, 6(1), 61–83. <https://doi.org/10.1177/107754630000600104>
- Carrasco, J., Baños, A., & Schaft, A. (2010). A passivity-based approach to reset control systems stability. *Systems Control Letters*, 59, 18–24. <https://doi.org/10.1016/j.sysconle.2009.10.009>
- Cazzulani, G., Resta, F., Ripamonti, F., & Zanzi, R. (2012). Negative derivative feedback for vibration control of flexible structures. *Smart Materials Structures - SMART MATER STRUCT*, 21. <https://doi.org/10.1088/0964-1726/21/7/075024>
- Chen, L., He, F., Sammut, K., & Cao, T. (2002). Nonlinear active vibration absorber design for flexible structures. *Proceedings of the International Conference on Control Applications*, 1, 321–326 vol.1. <https://doi.org/10.1109/CCA.2002.1040206>
- Clegg, J. C. (1958). A nonlinear integrator for servomechanisms. *Transactions of the American Institute of Electrical Engineers, Part II: Applications and Industry*, 77(1), 41–42. <https://doi.org/10.1109/TAI.1958.6367399>
- Deenen, D., Heertjes, M., Heemels, W., & Nijmeijer, H. (2017). Hybrid integrator design for enhanced tracking in motion control. *2017 American Control Conference (ACC)*, 2863–2868. <https://doi.org/10.23919/ACC.2017.7963385>
- Guo, Y., Wang, Y., & Xie, L. (2009). Frequency-domain properties of reset systems with application in hard-disk-drive systems. *IEEE Transactions on Control Systems Technology*, 17(6), 1446–1453. <https://doi.org/10.1109/TCST.2008.2009066>
- Guo, Y., Xie, L., & Wang, Y. (2015). *Analysis and design of reset control systems*. <https://doi.org/10.1049/PBCE094E>
- Heertjes, M., van den Eijnden, S., Sharif, B., Heemels, M., & Nijmeijer, H. (2019). Hybrid integrator-gain system for active vibration isolation with improved transient response [8th IFAC Symposium on Mechatronic Systems MECHATRONICS 2019]. *IFAC-PapersOnLine*, 52(15), 454–459. <https://doi.org/https://doi.org/10.1016/j.ifacol.2019.11.717>

- HOROWITZ, I., & ROSENBAUM†, P. (1975). Non-linear design for cost of feedback reduction in systems with large parameter uncertainty. *International Journal of Control*, 21(6), 977–1001. <https://doi.org/10.1080/00207177508922051>
- Kim, S.-M., & Oh, J.-E. (2013). A modal filter approach to non-collocated vibration control of structures. *Journal of Sound and Vibration*, 332(9), 2207–2221. <https://doi.org/https://doi.org/10.1016/j.jsv.2012.12.002>
- Nešić, D., Zaccarian, L., & Teel, A. R. (2008). Stability properties of reset systems. *Automatica*, 44(8), 2019–2026. <https://doi.org/https://doi.org/10.1016/j.automatica.2007.11.014>
- Olgac, N., & Holm-Hansen, B. (1995). Tunable Active Vibration Absorber: The Delayed Resonator. *Journal of Dynamic Systems, Measurement, and Control*, 117(4), 513–519. <https://doi.org/10.1115/1.2801108>
- Raimúndez, C., Barreiro, A., & Villaverde, A. F. (2011). Damping Injection by Reset Control [024504]. *Journal of Dynamic Systems, Measurement, and Control*, 134(2). <https://doi.org/10.1115/1.4005369>
- Saikumar, N., Heinen, K., & HosseinNia, S. H. (2021). Loop-shaping for reset control systems: A higher-order sinusoidal-input describing functions approach. *Control Engineering Practice*, 111, 104808. <https://doi.org/https://doi.org/10.1016/j.conengprac.2021.104808>
- Saikumar, N., Sinha, R. K., & HosseinNia, S. H. (2019). constant in gain lead in phase” element– application in precision motion control. *IEEE/ASME Transactions on Mechatronics*, 24(3), 1176–1185. <https://doi.org/10.1109/TMECH.2019.2909082>
- Vidyasagar, M. (1993). *Nonlinear systems analysis (2nd ed.)* Prentice-Hall, Inc.

5

CONCLUSION

In this thesis, a novel control technique was developed to improve transient response lightly damped structures. This was motivated by the ever-increasing demands for high-precision equipments that incorporate flexure-based elements. The resulting structural vibrations reduce their precision and increase settling times, leading to lower machine throughput and increased production times.

After having initially surveyed state-of-the-art linear active damping techniques, we realized that nonlinear hybrid control techniques held greater promise to improve transient damping characteristics. Reset control was chosen as preferred control technique due to its well-studied nature and the possibility to design reset controllers in the frequency-domain using describing functions.

We started off with the work of [Bupp et al., 1996], and extended it to a velocity feedback framework. This was motivated by the underlying physics, as it was shown that for damped plants, position feedback-based zero-crossing reset was ineffective. Extending the RVA structure into a velocity feedback framework, and translating this into frequency-domain characteristics using describing functions provided the basis for the synthesis of a novel reset-based bandpass filter, R_{bp} . This was designed by arranging two FOREs in parallel. Stability properties of this new reset bandpass filter and the closed-loop system were then analyzed using passivity-based techniques, developed specifically for reset control systems. Furthermore, rules-of-thumb were also provided for the rapid design of the novel bandpass filter using describing functions.

This Resetting Velocity Feedback (RVF) framework was then validated both numerically and experimentally. It was shown to provide a 273.1% increase in transient damping performance to a linear bandpass filter for the same control gain. Optimal transient damping performance was achieved for a dimensionless active damping ratio, $\zeta_{active} = 0.55$ as opposed to a HIGS bandpass filter which performed optimally at $\zeta_{active} = 1.0$ [Heertjes et al., 2019]. This shows that the RVF framework requires lower control gains, and is thus more energy efficient. Furthermore, the robustness of this reset bandpass filter was examined by performing sensitivity analysis. We saw that for a 10% variation in the tuning parameters, the reset bandpass filter still provided better transient damping

performance compared to the nominal linear bandpass filter. Finally, we showed that the reset bandpass filter can be modified to compensate for known system delays, which results in a transient damping performance comparable to the nominal case.

As future work, the study can be extended to more complex distributed parameter systems. Multiple (and non-collocated) modes may render the plant non-passive and affect stability. This could be a direction for future research. Presently, the controller is not explicitly designed to be robust to plant variations. An adaptive scheme can be incorporated into this framework to improve its performance in uncertain environments. The design of a robust version of the controller could also be explored. Finally, a theoretical treatment on the effect of delays on system performance is also left out. Further theoretical questions remain unanswered in these directions and could pave the way for interesting future research.

6

APPENDIX A

MATLAB FUNCTION: GENERATE R_{bp}

```
%Parameters for FORE
Ts = 100e-6; % Sampling Time
A = -31.4; % Pick A as eigenfrequency/2
B = -1*A;
C = 1;
D = 0;

%% Define element FORE 1
Fore1 = ss(0.8*A,0.8*B,C,D); % BLS of the reset element
Ar1 = 0.0;% Define reset law
Fore1d = c2d(Fore1,100e-6,'tustin'); % Discretize element
n = 1; % highest order of HOSIDF
freqs = logspace(-1,5,10000); % range of frequencies
GR1 = hosidfHeinen(Fore1, Ar1, n, freqs); % HOSIDF reset for comparison

%% %% Define element FORE 2
Fore2 = ss(1.5*A, 1.5*B, C, D); % BLS of the reset element
Ar2 = 0.0;% Define reset law
Fore2d = c2d(Fore2,100e-6,'tustin'); % Discretize element
n = 1; % highest order of HOSIDF
freqs = logspace(-1,5,10000); % range of frequencies
GR2 = hosidfHeinen(Fore2, Ar2, n, freqs);

%% FORE-based Bandpass
BP1 = 144.8*(GR2 - GR1); % pick the gain according to rule-of-thumb
```

```
%% Plotting DF
ln = 1;
clear leg
for iter = 1:2:size(BP1,1)
    bodeHOSIDF(BP1,freqs,iter);
    leg{ln} = sprintf(' n = %d',iter);
    ln = ln+1;
end
subplot(2,1,1)
legend(leg)
```

MATLAB FUNCTION: HOSIDFHEINEN.M

```
function [G] = hosidfHeinen(sys, Ar, n, freqs)
% Calculated the higher order describing function for a given reset
% system using the method of Kars Heinen
    % SYS is the reset element described in state space
    % AR is the amount of reset you want to achieve (typical 0)
    % N is the highest describing function order
    % FREQS contains the frequencies the describing function is calculated
    % for represented in rad/s
    % G is a matrix with HOSIDF orders as rows and freqs as columns
disp('hosidfHeinen')
G = zeros(n,length(freqs));

for iter = 1:n
    G(iter,:) = hosidfcalc(sys, Ar, iter, freqs);
end
end
```

MATLAB FUNCTION: BODEHOSIDF.M

6

```
function [] = bodeHOSIDF(G, freqs, n)
%bodeDF Plots a HOSIDF bode plot up to order N
mg = 20*log10(abs(G)); % magnitude
pg = 180*angle(G)/pi; % phase
orders = n;
% for iter = 1:length(orders)% generate legend
%     leg{iter+1}=sprintf('DF = %d',orders(iter));
% end
% figConfig()
% figure() ; %clf;
subplot( 2 , 1 , 1 ) ;
semilogx(freqs,mg(orders,:), '-'); % plot only odd orders
hold on
grid on;
ylabel( '$|\cdot|$ [dB]' ) ;
subplot( 2 , 1 , 2 ) ;
semilogx(freqs, pg(orders,:), '-'); % plot only odd orders
hold on
grid on;
xlabel( '$\omega$ [rad/s]' ) ;
ylabel( '$\phi(\cdot)$ [deg]' ) ;
end
```

MATLAB FUNCTION: HOSIDFCALC.M

```

function [G] = hosidfcalc(sys, Ar, n, freqs)
    % Calculates the describing function of a reset system
    % SYS is the reset element described in state space
    % AR is the amount of reset you want to achieve (typical 0)
    % N is the describing function order
    % FREQS contains the frequencies the describing function
    % is calculated for represented in rad/s
    % Kars Heinen - TU Delft - 2017

    % to do; replace inv() by 'matlab \'

    % odd orders will be skipped
    if (mod(n,2) == 0)
        G = 0;
        return;
    end
    A = sys.a; B = sys.b; C = sys.c; D = sys.d;
    G = zeros(1,numel(freqs));

    for i=1:numel(freqs)
        w = freqs(i);

        Lambda = w*w*eye(size(A)) + A^2;
        LambdaInv = inv(Lambda);

        Delta = eye(size(A)) + expm(A*pi/w);
        DeltaR = eye(size(A)) + Ar*expm(A*pi/w);

        GammaR = inv(DeltaR)*Ar*Delta*LambdaInv;
        ThetaD = (-2*w*w/pi)*Delta*(GammaR-LambdaInv);

        if (n==1)
            G(i) = C*inv(j*w*eye(size(A)) - A)*(eye(size(A)) + j*ThetaD)*B;
        else
            G(i) = C*inv(j*w*n*eye(size(A)) - A)*j*ThetaD*B;
        end
    end

    if (n == 1)
        G = G + D;
    end
end
end

```

MATLAB CODE: IMPORT LABVIEW DATA AND GENERATE FRF OF PLANT

```

clear all; close all; clc

%% Import the data from LabVIEW's LVM file
measurement = lvm_import('sens25run1.lvm');

%% Generate time grid
t = linspace(0,37.5,length(measurement.Segment1.data(:,5)));

%% Plot Actuator and Sensor signals
figure(); sgtitle('Patch Actuation')
subplot(6,1,1); plot(t,measurement.Segment1.data(:,2));
title('Actuator 1 Input');

subplot(6,1,2); plot(t,measurement.Segment1.data(:,3));
title('Actuator 2 Input');

subplot(6,1,3); plot(t,measurement.Segment1.data(:,4));
title('Sensor 1 Output');

subplot(6,1,4); plot(t,measurement.Segment1.data(:,7));
title('Sensor 2 Output');

subplot(6,1,5); plot(t,measurement.Segment1.data(:,6));
title('Sensor 3 Output');

%% Generate input and output vectors
u = measurement.Segment1.data(1:end,6); %Actuation
y1 = measurement.Segment1.data(1:end,7); %Displacement
y2 = measurement.Segment1.data(1:end,4); %Velocity

%%
nfs = .5e5; N = 1e5; Fs = 1/100e-6;
wind = hann(N);

%% Force-Velocity FRFs
[txy2,ft2] = tfestimate(u,-1*y2,wind,[1],nfs,Fs);
coherence2 = mscohere(u,-1*y2,wind,[1],nfs,Fs);

figure(); sgtitle('Transfer Function from Lorentz actuator to LDV')
subplot(3,1,1); semilogx(ft2(1:end),20*log10(abs(txy2(1:end))));
title('Magnitude'); xlabel('f (Hz)'); ylabel('Gain (dB)'); grid

```

```
subplot(3,1,2); semilogx(ft2(1:end),(180/pi*angle(txy2(1:end))));  
title('Phase'); xlabel('f (Hz)'); ylabel('degree'); grid
```

```
subplot(3,1,3); semilogx(ft2(1:end),(coherence2(1:end)));  
title('Coherence'); xlabel('f (Hz)'); ylabel('Coherence'); grid;  
ylim([0 1.1]);
```

```
%% Fit Transfer Function to experimental FRF
```

```
f1 = 1*round(1*length(ft2)/5000);  
f2 = 10/25*round(50*length(ft2)/5000);  
sys = frd(txy2(50:300),2*pi*ft2(50:300));  
system = tfest(sys,2,1);  
[num,den] = tfdata(system);  
ftf = tf(num,den);  
bode(system);
```

```
%% Fitted Transfer Function
```

```
s = tf('s');  
Ccont = (800*s)/((s+8)*(s+800)); % generate linear bandpass  
Cd = c2d(Ccont,100e-6,'tustin'); % discretize linear bandpass  
bode(Ccont);  
hold on
```

7

APPENDIX B

The experimental setup consists of:

- Single DOF flexure stage
- Lorentz Actuator
- Laser Doppler Vibrometer (Polytec OFV-505) – Velocity Sensor
- Current Source Amplifier with Amplification Factor 0.0625 A/V
- Dual Power Supply (12V - 1A) for the amplifier
- compactRIO FPGA controller

The setup is schematically shown in the Figure 7.1.

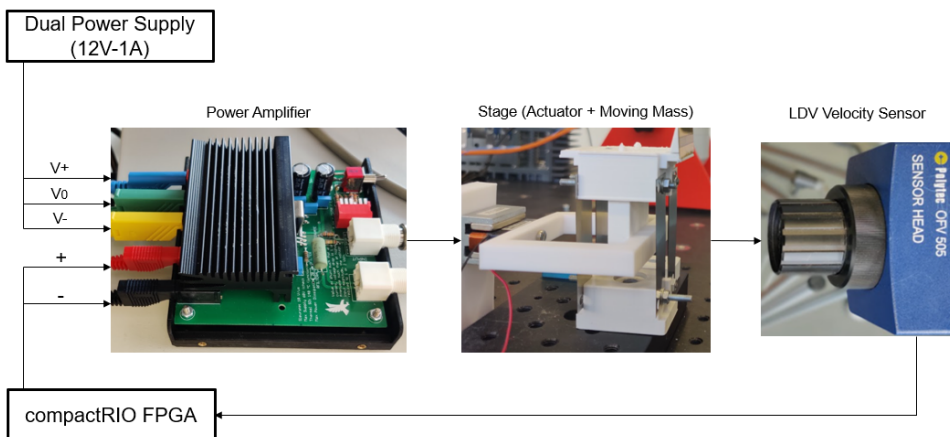


Figure 7.1: Experimental setup

SINGLE DEGREE OF FREEDOM FLEXURE STAGE

The moving mass is 3D printed from PLA. The actuator is positioned to provide the force at the centre of rotation to eliminate moments, and results in an exactly constrained 1 DOF system. The four aluminium flexures are 0.2mm thick, 60mm long and 8 mm wide, and provides stiffness and low natural damping. They are clamped using bolts to the moving mass. On top of the moving mass is a reflective sticker to provide a suitable reflective surface to achieve high laser signal quality.

A practical tip: Ensure the eigenfrequency of the plant is well-chosen if you have the freedom to design your own plant. In this case, the eigenfrequency of 13.2 Hz is well suited for experiments, as it is high enough to avoid the high-pass characteristics of electrical wires, and low enough to be not affected by the low-pass characteristics of the power amplifier, noise, and the sampling frequency limits of the compactRIO.

LORENTZ ACTUATOR

The actuator is a moving-coil Lorentz actuator (ETEL 025C) designed to provide a peak force of about 3N. The underhung design provides linearity in the operating stroke of 2mm. It's a non-contact bearing less design, in which the structure mechanism acts like a bearing. This ensures zero friction in the actuator. ThorLabs fine-translation stages are used to position the moving part (coil) of the actuator w.r.t to the stationary part (magnets), and to ensure that the coil is completely underhung and centrally aligned. This should provide close-to-ideal actuator behaviour.

7

LDV VELOCITY SENSOR

A Polytec OFV-505 LDV is used to acquire absolute vibration velocity signals. An LDV provides voltage signals proportional to the vibration velocity by utilizing Doppler effect. This eliminates the need to differentiate position signals or integrate acceleration signals, and eases implementation. The LDV control panel offers tune-able sensor sensitivity. For this study a sensitivity of 25 mm/s/V is used. A lower sensitivity was found to show clipping, as the DAQ system was limited to +/- 10V signals. Depending on the magnitude of vibration velocities, a lower or higher sensitivity can be chosen, if higher/lower signal resolutions are desired.

CURRENT-SOURCE POWER AMPLIFIER

In a physical system the amplifier converts the low-voltage, low-current control signal output of the D/A-converter into the electrical current output necessary in the actuator. Since it is desired to control the force of the Lorentz actuator, and the force is proportional to the current, a current source amplifier is selected. This amplifier has a linear behaviour and is able to provide a bi-directional current in order to generate a bidirectional force. The inductive load of the coil works as a low pass filter, resulting in a decreasing current output at higher frequencies. Using current feedback results in an output current independent of the frequency dependent impedance of the actuator. The decreasing currents at high frequencies are compensated by applying a higher output

voltage. In Figure 7.2 a simplified schematic of the amplifier is shown.

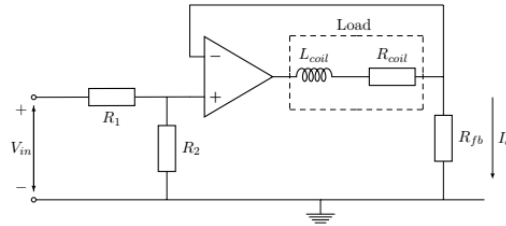


Figure 7.2: Current-source amplifier design

The amplification factor can be selected by choosing the appropriate resistances, according to

$$\frac{I_0}{V_{in}} = \frac{R_2}{(R_1 + R_2) R_{fb}} \quad (7.1)$$

In this particular case, the resistances are chosen such that $\frac{I_0}{V_{in}} = 0.0625$ A/V. This should be chosen according to the magnitude of the voltage output of the DAC, and the current limit of the actuator.

The op-amp used in the amplifier is an OPA548 by Texas Instruments. Following the rated voltage and current limits for this op-amp, a Dual Power Supply of 12V-1A is used for powering the amplifier.

It is important to ensure that the dynamic behaviour of the amplifier does not affect the dynamics of the plant. In this case, at the eigenfrequency of the plant (13.2 Hz), the amplifier provides constant gain and 0 phase, as its cut-off frequency is 10 kHz.

COMPACTRIO FPGA CONTROLLER

compactRIO by National Instruments is an FPGA, which can run acquire signals (ADC), compute control actions with these signals, and provide the necessary voltage signals to the amplifier via a DAC. The compactRIO chassis has a modular design. Depending on the nature of your sensor signals, you can choose either Analog Input (AI) or Digital Input (DIO) modules to acquire sensor data. Similarly, an Analog Output (AO) module can give output signals to the amplifier/actuator. For these particular experiments, AI module with BNC connector (NI 9215) is used to acquire the LDV signals. The control signals are sent out through the AO module (NI 9264).

The compactRIO interfaces with the host computer using LabVIEW, a software by National Instruments. A basic guide to setup a LabVIEW FPGA programming environment is highlighted next.

LABVIEW

LabVIEW 2020 (32-bit) was used in the experiments. Please note that even if the computer runs a 64-bit OS, LabVIEW 2020 (32-bit) was more stable and interfaces perfectly with the compactRIO and other software modules.

INSTALLATION

Install LabVIEW 2020 (32-bit) and the following compatible modules from NI.com:

LabVIEW RealTime Module

LabVIEW FPGA Module

LabVIEW Control and Simulation Module

LabVIEW MathScript Module

NI compactRIO

CONNECTING COMPACTRIO TO THE HOST COMPUTER

Connect the compactRIO to the computer using the USB cable. Make sure all hardware AI/AO modules are inserted correctly in the compactRIO before connecting to the computer

NI MAX should automatically open. Check if the compactRIO is recognized in the "Remote Systems" tabs. If it is not recognized, it means that the compactRIO does not have operating software installed in it. If this is the case, check NI documentation for help on how to install this.

Once NI MAX recognizes the connected compactRIO, we are ready to open LabVIEW and interface it with compactRIO

Open up a Blank Project in LabVIEW. On the Project page we need to add a target (i.e., the compactRIO) to the project to perform real-time control and computation on the compactRIO by interfacing it with the computer.

Right-click the Project Title ("Untitled Project") on the project tree and select "New > Targets and Devices". Select "Discover an existing target or device" and select the Real-Time CompactRIO from the list of targets, as shown in Figure 7.3.

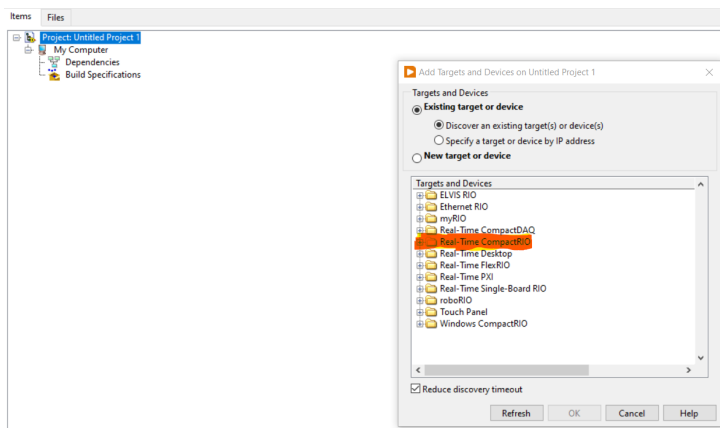


Figure 7.3: Adding the FPGA compactRIO target to your LabVIEW project

Once you select the appropriate compactRIO target, LabVIEW will add it to the LabVIEW Project. When prompted to select a mode to run the target in, choose "LabVIEW FPGA Interface". Once target addition is complete, a new component will appear in the Project Tree: "NI-cRIO-<serial-number> (IP address)".

Once this appears, expand the CRIO tree until you see the FPGA target. Expand this further until you see the modules listed. Ensure that all physical AI/AO modules are visible in this drop-down list, with the slot number indicated correctly. **Right-click on ALL of these modules, and select “Properties”.** In the Module Properties window, set Calibration Mode to “Raw”, as shown below in Figure 7.4. This step is crucial. If the mode is not set to Raw, the acquired signals and the output signals will behave weirdly, and the experiments will be ineffective.

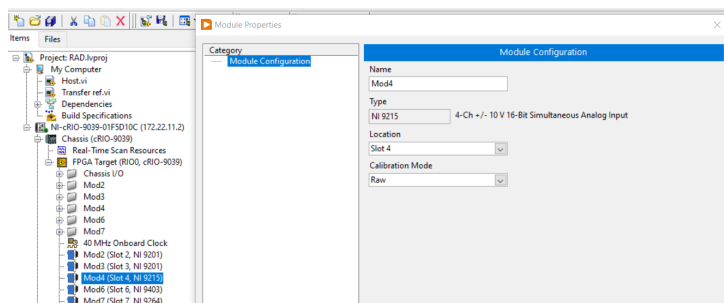


Figure 7.4: Choosing Raw calibration mode for AI/AO modules

Once these steps are carried out, we are ready to program the FPGA to acquire signals, compute control actions, and send the control signal out through the AO modules.

LABVIEW FPGA PROGRAM STRUCTURE

Figure 7.5 shows a typical LabVIEW FPGA project structure.

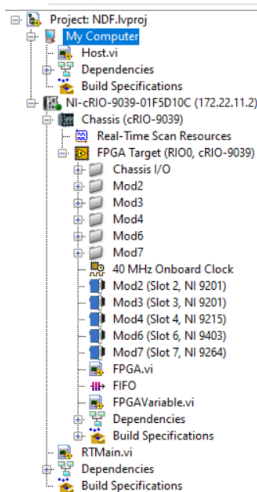


Figure 7.5: LabVIEW FPGA program structure

Host VI: This VI is part of the “My Computer” section of the project tree. This VI usually deals with writing the acquired sensor data to an LVM file, which can be later processed in MATLAB for data visualization.

RTMain VI: This VI interfaces the host computer with the FPGA. It is responsible for transferring the data from FPGA VI to the Host VI. Furthermore, RTMain VI is used to control the program, through the LabVIEW control panel window. Running the RT Main VI initiates the test, and provides the signals, which in-turn runs the FPGA VI. Tuning parameters for the controller, and other user-tuneable test parameters such as frequency of the excitation, amplitude of the excitation, etc are part of RT Main, and can be changed in real-time through the front panel, by the user.

Both Host and RTMain are run on the host computer and are hence not the fastest in execution.

FPGA VI: This VI houses the actual code, to acquire signals, compute controller action, and send the control signals to the actuator. This is run on the dedicated FPGA processor and is therefore extremely fast. A problem with this is that every time something in the code changes, the FPGA code needs to be recompiled and could take anywhere from 20 minutes to one hour. It is therefore better to only provide the logic of the algorithms in the FPGA VI, and the parameters (like frequency, amplitude, control gains, coefficients of transfer functions etc) in the RTMain VI which is then linked to the FPGA VI. This way re-compilation of the FPGA VI is avoided every time the user wishes to modify the controller parameters, or values of certain test variables.

FIFO: First-In-First-Out is a stack array to enable enough buffer to compensate for the execution speed discrepancies of the compactRIO and the host computer. The FIFO should be configured as shown in the Figure ??.

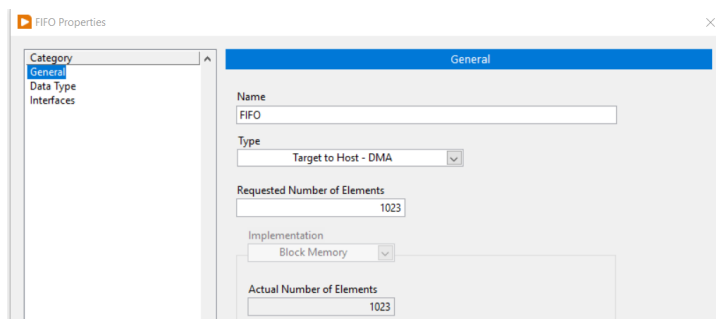


Figure 7.6: Setting up FIFO

EXPERIMENTAL METHOD

To focus on controller validation, the physical system is chosen to be a simple single degree-of-freedom flexure stage. The moving mass is 3-D printed from PLA, and the flexures provide the stiffness and (low) natural damping to the system. A Lorentz actuator (ETEL 025C) is used to provide both, the disturbance signal and the control force. The actuator is positioned at the midpoint of the flexures to eliminate the undesired rotation of the stage to a moment. This ensures that the five degrees-of-freedom of the stage are constrained. A Polytec OFV-505 Laser Doppler Vibrometer (LDV) is used as a velocity

sensor, which provides voltage signals proportional to the vibration velocity. National Instruments compactRIO FPGA is used to acquire the signals, and compute and deliver the control signal to the amplifier. LabVIEW 2020 32-bit is used to interface the host computer with compactRIO and DAQ systems. The amplifier used is a current-source amplifier that uses an OPA548 op-amp by Texas Instruments. By designing a suitable circuit, it can provide a constant amplification factor of 0.0625 A/V from 5Hz until high frequencies.

Before designing the controller, system identification is performed by exciting the system with a chirp (swept sine) signal from 0.5 Hz to 300 Hz. Using MATLAB's System Identification Toolbox, the Frequency Response Function (FRF) of the system is obtained. A transfer function is fitted to the experimental data to capture the single mode of interest using MATLAB's `tfestimate` function (see Appendix A)

With the plant parameters identified experimentally, the controller can be designed according to the rules-of-thumb. As this is to be implemented on a digital control system, the controller in state-space form is discretized using the `c2d` MATLAB function, with the `'tustin'` option enabled (see Appendix A). A discrete linear bandpass can also be designed similarly. The sampling frequency is chosen to be 10 kHz, which is significantly higher than the eigenfrequency to avoid aliasing, but well within the limits of the FPGA's computational power (40 MHz digital clock). Before deploying the discrete controller on the experimental setup, it is numerically simulated using Simulink (solver: `ode4`, fixed time-step: `1e-4`). To increase the credibility of the simulations, the control signals and plant outputs are quantized, and Zero Mean White Noise (ZMWN) is added to the plant output to model sensor noise. The results of these can be found in Section 4.4.